EE 408: Power Electronics Design: Final Report Grading and Evaluation Sheet (Simulation-Based Design)
University of Alaska Fairbanks
Electrical and Computer Engineering Department
Spring 2020

EE 408/608: Power Electronics Design	Project Final Report (Simulation-Based Design):	Total:	150.00

Team Members:	1) Nick Wirak 2) Tushar Biswash 3) Avro Mozumder	TEAM MEMBER(s) Responsible (Name)

		Name	% Effort	List Subsections for Team Member
Title Page (Project Title, Course, Team Member Names & Emails, Date Submitted):	0.5	Nick	100	
Pres/ Format:	0.17			

		Name	% Effort	List Subsections for Team Member
Table of Contents (Follow Template including List of Figures and List of Tables):	2	Nick	100	
Pres/ Format:	0.67			

		Name	% Effort	List Subsections for Team Member
Abstract (Follow Example):	5	Nick	100	
Pres/ Format:	1.67			

		Name	% Effort	List Subsections for Team Member
Introduction (Objective, Background, Brief Intro to Your Design, Expected Outcome Summary Statement):	5	Nick	100	
Pres/ Format:	1.67			

		Name	% Effort	List Subsections for Team Member
Design (Design Description with Block Diagram, Design Requirements, & Explanation of Complete Circuit divided into Subsections with Schematics):	20	Tushar	100	everything else
		Nick	100	2.1 , 2.2 , 2.3.2.2 , 2.3.4 ,
		Avro	100	pwm circuit
Pres/ Format:	6.67			

		Name	% Effort	List Subsections for Team Member
Engineering Standards (IEEE 519, 299, & any Other Standards with Reference to Your Design with Discussion: Special Section of WPR #3 and #9):	5	Tushar	100	everything else
		Nick	100	usb paragraph
Pres/ Format:	1.67			

EE 408: Power Electronics Design: Final Report Grading and Evaluation Sheet (Simulation-Based Design)
University of Alaska Fairbanks
Electrical and Computer Engineering Department
Spring 2020

		Name	% Effort	List Subsections for Team Member
Critical Technological Challenges (Current Critical Design Challenges: Special Section of WPR #5 and #11):	5	Avro	100	
		Pres/ Format:	1.67	
Engineering Constraints (Design Constraints and Engineering Tradeoffs Faced in Design Project with Explanation & Discussion: Special Section of WPR #6 and #12):	5	Tushar	100	
		Pres/ Format:	1.67	
Societal Effects of Design (Societal Effects of Design Project with Explanation & Discussion: Special Section of WPR #4 and #10):	5	Nick	100	
		Pres/ Format:	1.67	
PSpice Simulations (Circuit schematics and analysis plots used in the design process divided into the Circuit Subsections with Explanation of Results & Discussion):	10	Tushar	100	everything else
		Nick	100	gate drive, 3.3.1 subsection
		Avro	100	3.3
		Pres/ Format:	3.33	
Simulation Test Results (Results including analysis and measurements over the intended range of operation Subdivided into Circuit Subsections with Observations, Explanations of Results and Discussion):	15	Tushar	100	everything else
		Nick	100	gate drive, 4.3.1 subsection
		Avro	100	4.3
		Pres/ Format:	5.00	
Final Component List and Budget (Table Subdivided into the Sections of the Circuit with Brief Description and Statement of Budget):	5	Nick	100	
		Pres/ Format:	1.67	
Workplan (Project Schedule as Gantt Chart from WPR #1 and #7, Discussion of Divided Tasks & Final Project Status):	5	Nick	100	
		Pres/ Format:	1.67	

EE 408: Power Electronics Design: Final Report Grading and Evaluation Sheet (Simulation-Based Design)
University of Alaska Fairbanks
Electrical and Computer Engineering Department
Spring 2020

		Name	% Effort	List Subsections for Team Member
IEEE Code of Ethics Considerations (Reference to your Design; include actual IEEE Code of Ethics in Appendix: Special Section of WPR #2 and #8)	5	Nick	100	
		Pres/ Format:	1.67	
Conclusions (Summarize Results, Briefly Discuss Design Problems, & Provide Possible Solutions):	10	Name	% Effort	List Subsections for Team Member
		Nick	100	
		Pres/ Format:	3.33	
References (Listed in Order of Appearance in Body with Proper Reference Format (see Template)):	2.5	Name	% Effort	List Subsections for Team Member
		Nick	4/10	
		Tushar	3/10	
		Avro	3/10	
		Pres/ Format:	0.83	
Report Integration, Editting, and Proofreading:	10	Name	% Effort	
		Nick: integration, self proof reading, limited other editing		
		Tushar; self proof reading		
		Avro: self proof reading		
Presentation/Format (Section Headings, Figure and Table Captions, Orphan/Widow, Spelling, Grammar, & Neatness):		Total Pres/ Format:	35.00	
Technical Points: Points for technical content.		Total Technical:	105.00	

Senior Design Draft Final Project Report: 5 and 12 Volt Solar Battery Chargers with Maximum Power Point Tracking

EE 408/608: Power Electronics Design

Design Team Members:

Tushar Biswash, stushar@alaska.edu

Avro Mozumder, umozumber@alaska.edu

Nick Wirak, nowirak@alaska.edu

Date: May 1, 2020

Contents

List of Figures

List of Tables

ABSTRACT

Solar energy harvested by photovoltaic (PV) cell arrays can be a convenient and accessible source of energy. It is increasingly used to augment local energy needs on the grid, as well as provide otherwise unattainable electricity off the grid. The energy captured by PV arrays must be transferred to batteries of various types for further storage and use. 5 and 12 Volts are common battery voltage standards that service many vehicular and home/personal electronics devices. The proposed system, presented in simulation, will function as a battery charger for these devices, converting the nominal 17.5 Volt output from a common solar PV module to usable levels. Cascaded buck-converters will be used to sequentially reduce voltage levels to 12 and then 5 Volts. In doing so, a Maximum Power Point Tracking (MPPT) algorithm and associated control circuitry will additionally be utilized for maximal power transfer from PV cells to battery elements. The complete system should form a stable, efficient, and self-contained 5 or 12 Volt battery charger that is safe for the batteries themselves.

1. Introduction

The objective of this design project was originally to create a working prototype (bread-boarded) circuit that transfers energy from a solar panel to batteries of various types. In the midst of the semester long project, the COVID-19 response disrupted the original plans and relegated the project to termination at the simulation stage. We identified 12 V lead-acid and 5 V lithium-polymer (LiPo) batteries as circuit loads, as they are common in availability and utilization. 12 V batteries are used during internal-combustion engine starting cycles, and also as general DC sources (deep cycle RV or marine batteries). 5 V LiPo batteries are ubiquitous in consumer electronics, especially tablets and smartphones.

The Kyocera KC85T 85 W solar PV module served as a model source for our design. It offers the minimum power requirements for 12 V battery charging, and was directly available to us as a legacy item (from the University of Alaska-Fairbanks (UAF): it is no longer easily found in stock). In this case, buck converters are the preferable DC-DC converters for their function and simplicity, although in some cases, combinations of solar PV module specifications and battery charging requirements could necessitate the use of buck-boost converters.

We had intended to use a microcontroller with onboard PWM and ADC capabilities as the control unit, as opposed to analog circuitry during circuit implementation. This control strategy was adapted and incorporated into a series of MATLAB® simulations. The microcontroller made the design completion simpler, and also provided more control over circuit behavior using digital logic. Using digital logic and common microcontroller capabilities, we can provide adequately conditioned power signals to 12 and 5 V batteries from an 85 W solar panel. We have furthermore demonstrated maximum-power-point tracking (MPPT) to accommodate maximal circuit loading given suboptimal solar PV module (simulated) environmental operating conditions.

2. Design

This section will cover the overview and details of the design, and is divided into seven sub-sections. The first subsection introduces the requirements imposed on the design, and the second subsection presents the basic system block diagram that we propose to meet those requirements. Subsequent sections include additional details of the design. Later subsections discuss engineering standards of battery chargers, critical technological challenges faced in the design process, additional engineering constraints, and hypothetical effects of the design on society.

2.1. Design Requirements

Table 1 shows project design requirements in the approximate form of a requirements traceability matrix (RTM).

***Table 1**: Requirements traceability matrix showing design requirements.*

Item #	Category	Description
1	General	The design will be an electrical power conversion device capable of being fed from an unregulated 12-24 V DC source.
2	General	The design will be capable of charging one 12 V DC lead-acid battery.
3	General	The design will be capable of charging at least one 5 V DC small electronic device via USB connection.
4	General	If a solar cell array module is used as a source, MPPT should be implemented for maximum energy delivery.
5	General	The design will be in compliance with relevant standards and codes.
6	Time	The design and simulation results must be presented on Wednesday, April 29, 2020.
7	Practical	A Kyocera KC85T 85 W solar PV module will be considered as a power source.

Beyond the requirements organized within the table, there are several other capabilities that we would like our design to have, should it be physically realized. We would like our design to be able to measure the battery and react accordingly. The charging sequence of the 12 V DC

battery involves continuous and constant application of between 14.6 to 14.8 V DC until the time that it becomes fully charged. The state of charge of the battery can be determined approximately by its open circuit voltage. After the battery becomes fully charged, float voltage (13.6 – 13.8 V DC) should be applied to prevent damage to the battery and maintain charge level. We would also like to ensure that discharging of batteries does not occur when the solar PV module voltage level drops. If the design can accommodate the load well, we would like to be able to source charging power to multiple 5 V devices for convenience. It is noted that simultaneous charging of a 12 V battery and 5 V batteries would be convenient, but impossible, given the power rating of the particular solar PV module that we have designed this project to use.

2.2. Basic Block Diagram

Figure 2.1 contains a basic block diagram of the proposed system. A solar PV module will source power for the system. Buck converters form the functional backbone for the design, converting solar PV module voltage to usable battery charging levels. The control logic unit controls the voltage conversion, and inputs include converter output and battery state (condition). The MPPT unit may be considered separately from the control unit, and provides an additional control element that attempts to optimize power delivery to the batteries. The PWM generator is a standalone subsystem that is often included as a functional unit in commercially available control systems, but provides an analog control signal that is disseminated via gate-drive units to the buck converters. A voltage regulator is included in the block diagram as a necessary element for circuit realization that feeds voltage controlled power to the control system. This system proposal will strictly be simulated for performance evaluation. Consequently, subsystems related to control elements will not necessarily be given a full representation.

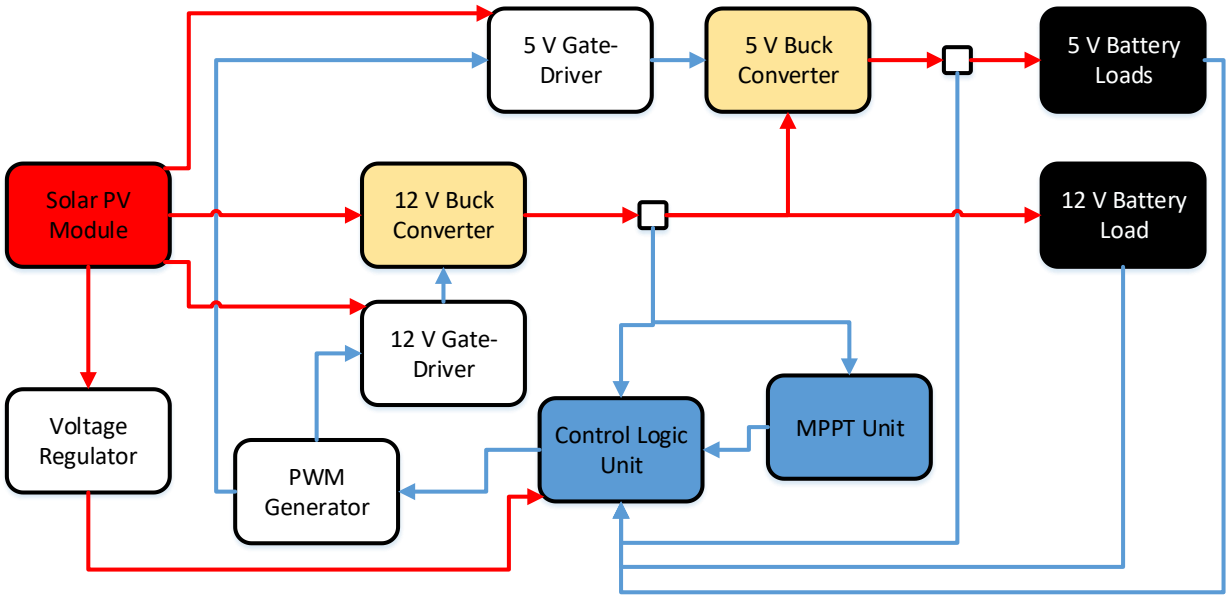

Figure 2.1: *System block diagram containing major subsystems. Red elements and signals represent power sources and signals. Blue elements and signals represent control (logic) sources and signals.*

2.3. Circuit Schematics

Figure 2.2 shows the circuit schematic of the buck converter for a 12 V and 5 V battery (shown in the figure as resistors). A solar PV module supplies power to charge both of the battery and feedback circuit maintains constant voltage across the battery terminals. The power delivered to the load is maintained at maximum value while observing the constraints of the battery.

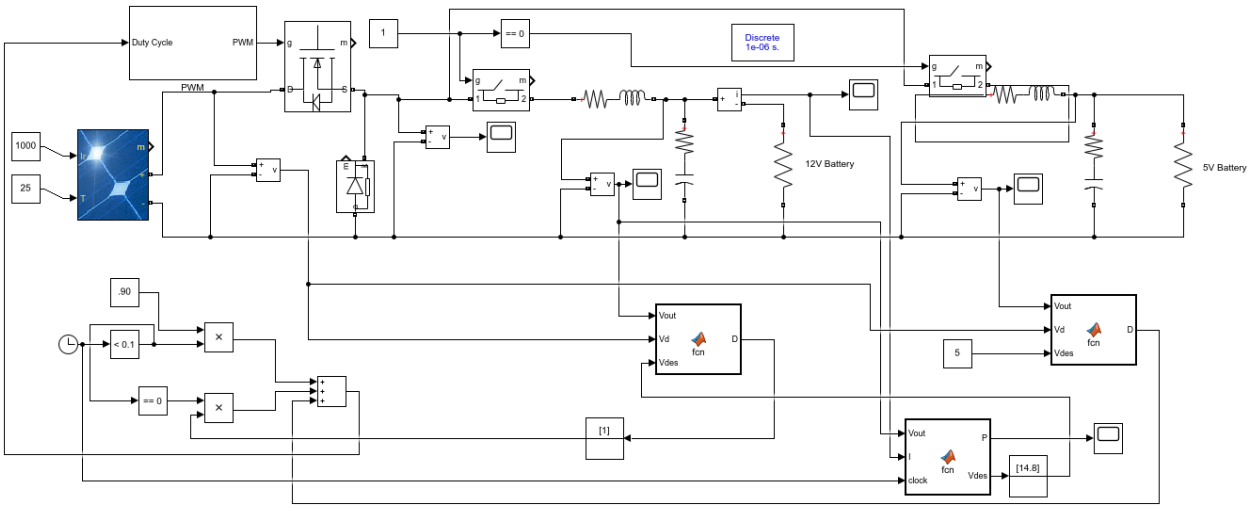

Figure 2.2: *Circuit schematic of 12 V and 5 V Battery charging system in MATLAB Simulink.*

2.3.1 PV Module:

PV module consists of a number of solar cells connected in series in order to produce required voltage and a number of cells in parallel to deliver the required current. One of the popular representations of the solar cell is a single diode model (*Figure 2.3*) [1] where internal loss in the cell is represented by the series resistance and leakage current is represented by the parallel resistance. The voltage (V) and the current (I) supplied to the load terminal can be expressed by the following equation (1):

$$I = I_{Ph} - I_0 \times \left(e^{\frac{V+I\times R_S}{a\times n_S \times V_T}} - 1 \right) - \frac{V+I\times R_S}{R_{sh}} \quad (1)$$

I_{ph} = Photon generated current
I_o = Saturation Current
n_s = Number of cells in series
R_s = Series Resistance
V_T = Thermal voltage
a = diode ideality factor

In this project, we have simulated the Kyocera KC85TS solar PV module which has an open circuit voltage of 21.7 V and a short circuit current of 5.34 A. The PV array Simulink block with parameters is shown in *Figure 2.4*. When customizing the Simulink solar module block for the Kyocera KC85TS, we obtained the graph for 1000 W/m^2 irradiance and 25˚C temperature (*Figure 2.5*).

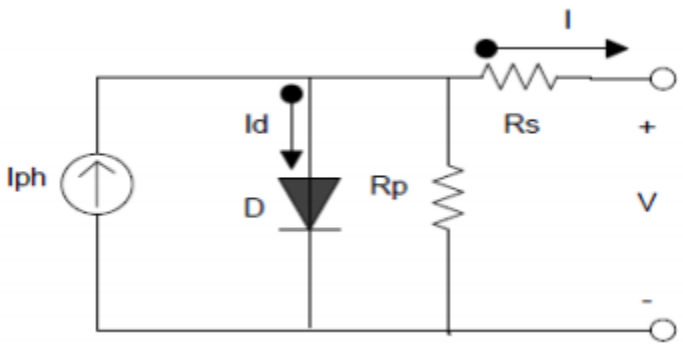

Figure 2.3: *Single diode model of a solar cell [1].*

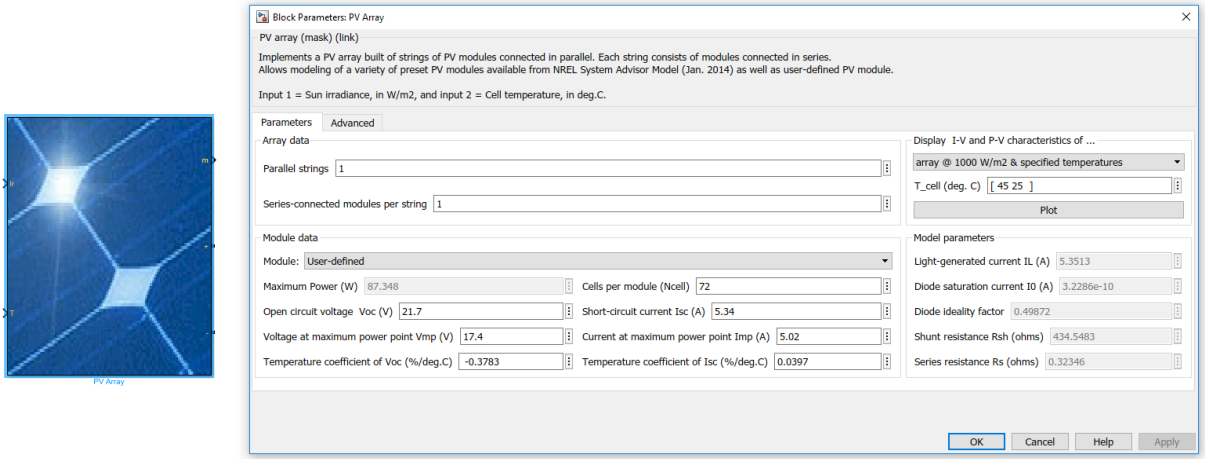

Figure 2.4: *Simulink PV array block with input parameters.*

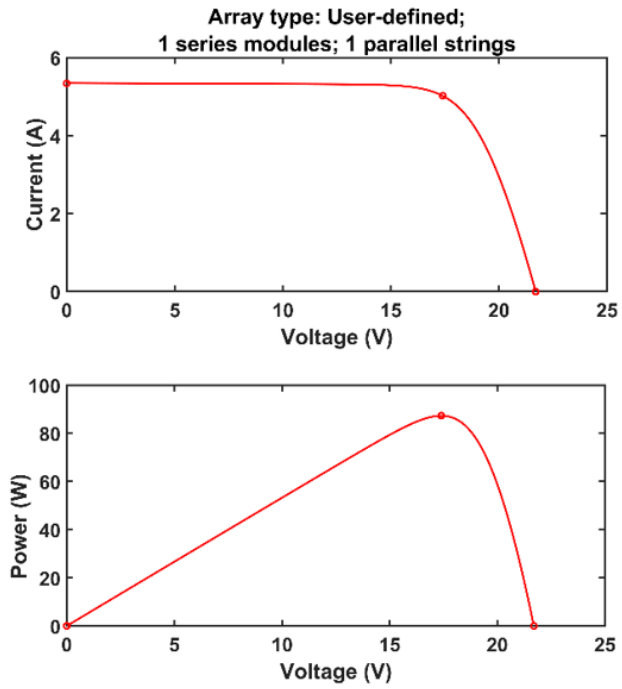

Figure 2.5: *I-V (top) and P-V (bottom) curve for Kyocera KC85TS solar module for 1000 W/m^2 irradiance and 25˚C temperature.*

2.3.2 Buck Converter

The buck converter mainly consists of a switching circuit (MOSFET), a diode and a LC filter. It needs some additional circuitry to make circuit operational.

2.3.2.1 PWM Circuit

Pulse width modulation (PWM) is a method of reducing the average voltage delivered by a source by changing the duty cycle of the pulse. This project is simulated in such a way so that a microcontroller will be used to generate PWM signals of desired frequency and duty ratio. The frequency will be kept fixed and duty cycle will be varied with the variation in input and circuit characteristics. *Figure 2.6* shows the Simulink block diagram of the PWM generator and signal of desired duty cycle produced by this PWM generator.

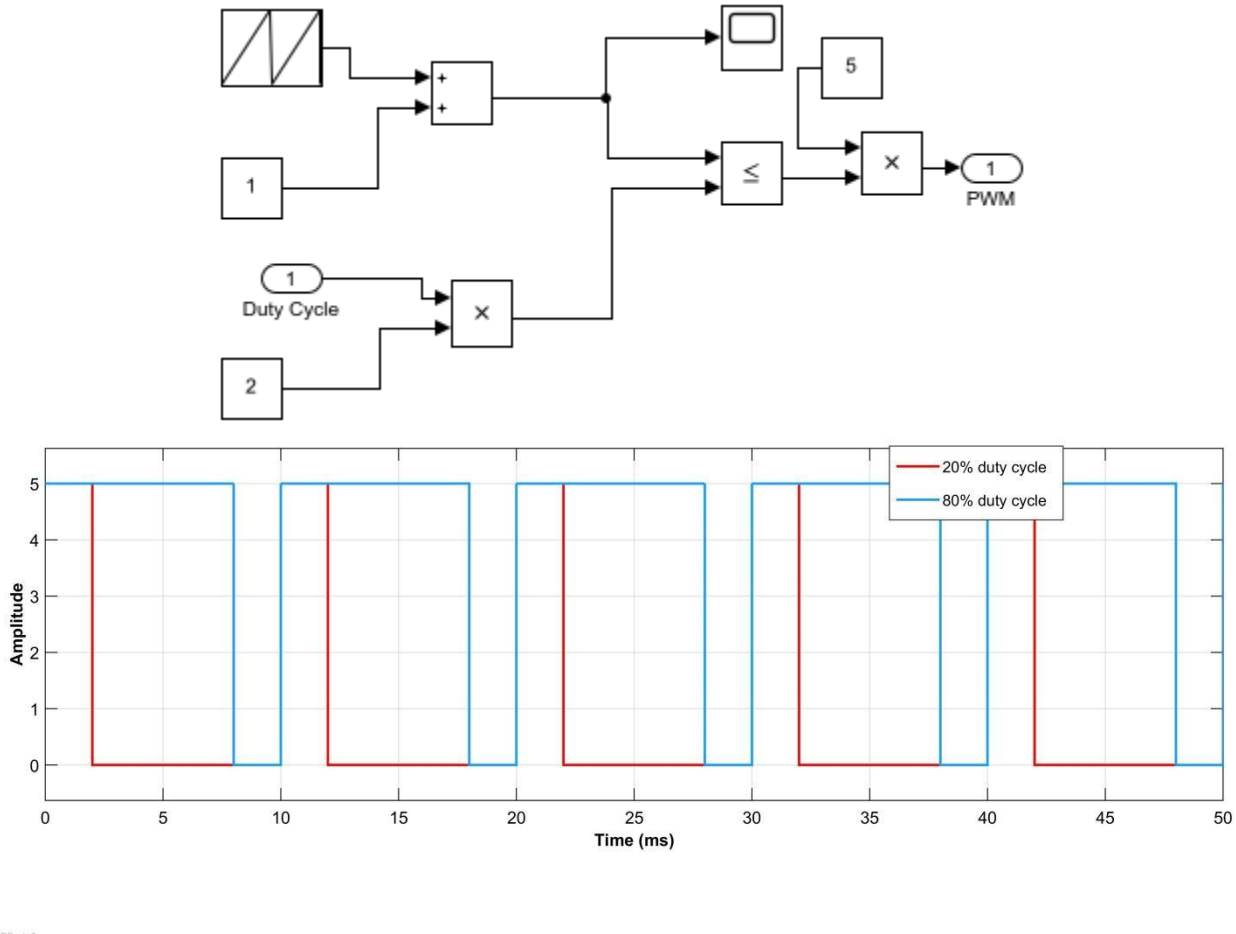

Figure 2.6: *(top) Simulink block diagram of the PWM signal generator (top). 20% and 80% duty cycles generated by the PWM (bottom).*

2.3.2.2 Gate Drive Circuit

Referring again to *Figure 2.1*, in a physical realization of the system, we propose the PWM Generator, Control Logic Unit, and MPPT Unit to be implemented with any of several common microcontrollers. The Arduino Uno Rev3 (see *Figure 2.7*) is a capable unit that incorporates the aforementioned components (as well as an ADC). Then in our design, PWM signals from an Arduino must be applied to the gates of power MOSFETs.

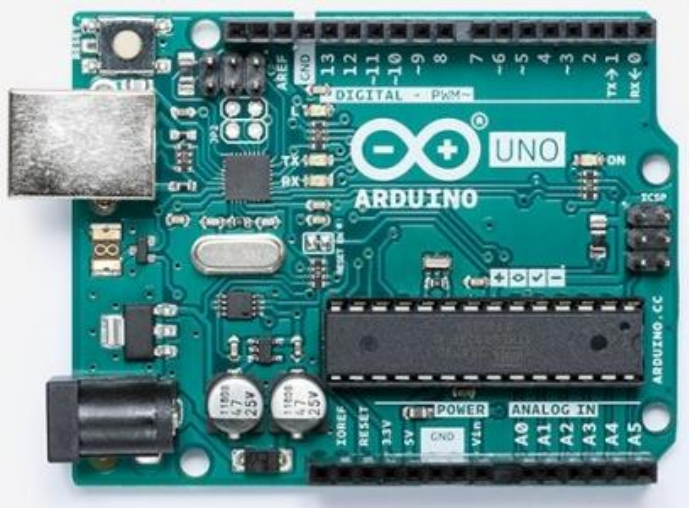

Figure 2.7: *The Arduino Uno Rev3 [2].*

The Arduino is capable of outputting 5 V on its GPIO pins, which should be a sufficient voltage to trigger the power MOSFETs that we could be utilizing in this design (see components in Section 5). As can be seen in the Arduino datasheet (see Appendix B.3) each GPIO pin should be able to supply a load with 20 mA. MOSFETs have significant transient current demands during the turn-on phase of operation due to their gate capacitance, and we do not expect the 20 mA from the Arduino to be able to meet those demands. It is even possible that subjecting the microcontroller to these high loads will damage it. The gate drive circuit is an intermediate element that can effectively function as a current amplifier for the Arduino. Also, being able to source more current than the Arduino can supply to the MOSFET should decrease its turn-on time.

We have considered three gate drive circuit configurations that are identical to those shown in class. Each circuit has certain advantages and disadvantages which demand a choice between simplicity and performance. *Figure 2.8* - *Figure 2.10* show the possible configurations. *Figure 2.8* shows a bipolar circuit implementation that utilizes both negative and positive voltage differentials along with a push-pull configuration to effectively transition the power MOSFET.

Evident from the schematic, *Figure 2.9* shows a simplified unipolar push-pull variant that does not make use of negative potential to encourage the PNP transistor to turn on. *Figure 2.10* contains a simple implementation that is reliant on a single NPN transistor. The first configuration gives the best performance and is the most complicated to implement. The second represents a middle ground where neither voltage potential is lost nor complicated boost circuitry is added. The third is the easiest to implement, but results in the least power MOSFET switching performance.

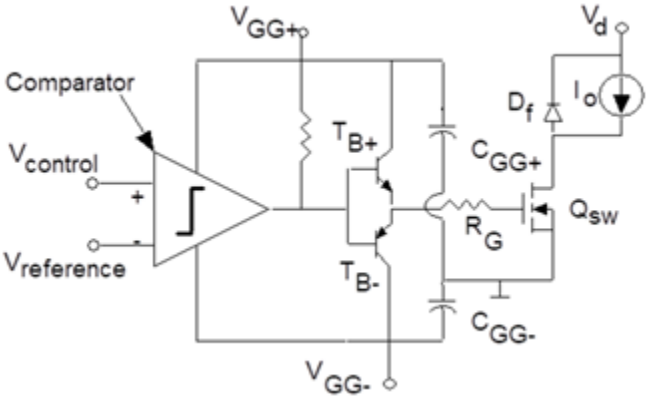

Figure 2.8: *Generic bipolar gate drive circuit (sourced from Lab 3 handout). The comparator functionality will be implemented with an Arduino.*

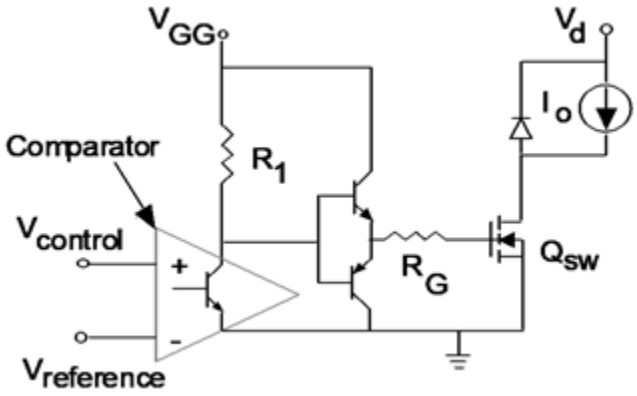

Figure 2.9**:** *Generic unipolar gate drive circuit (sourced from Lab 3 handout). The comparator functionality will be implemented with an Arduino.*

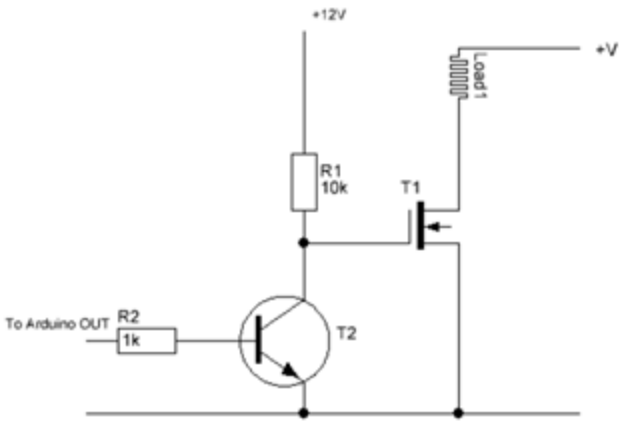

Figure 2.10: *Basic gate drive circuit using a single BJT (sourced from Lab 3 handout).*

2.3.2.3 Switching Circuit

An n-channel MOSFET can be used to switch the input voltage based on duty cycle of the PWM signal at the gate. When voltage at the gate goes high, voltage at the drain becomes equal to the input voltage and the MOSFET conducts. This ensures the input voltage pulse of frequency and duty cycle set by the PWM. On the contrary when voltage at the gate goes low, voltage at the drain goes to zero (shown in *Figure 2.11* with a duty cycle 87%).

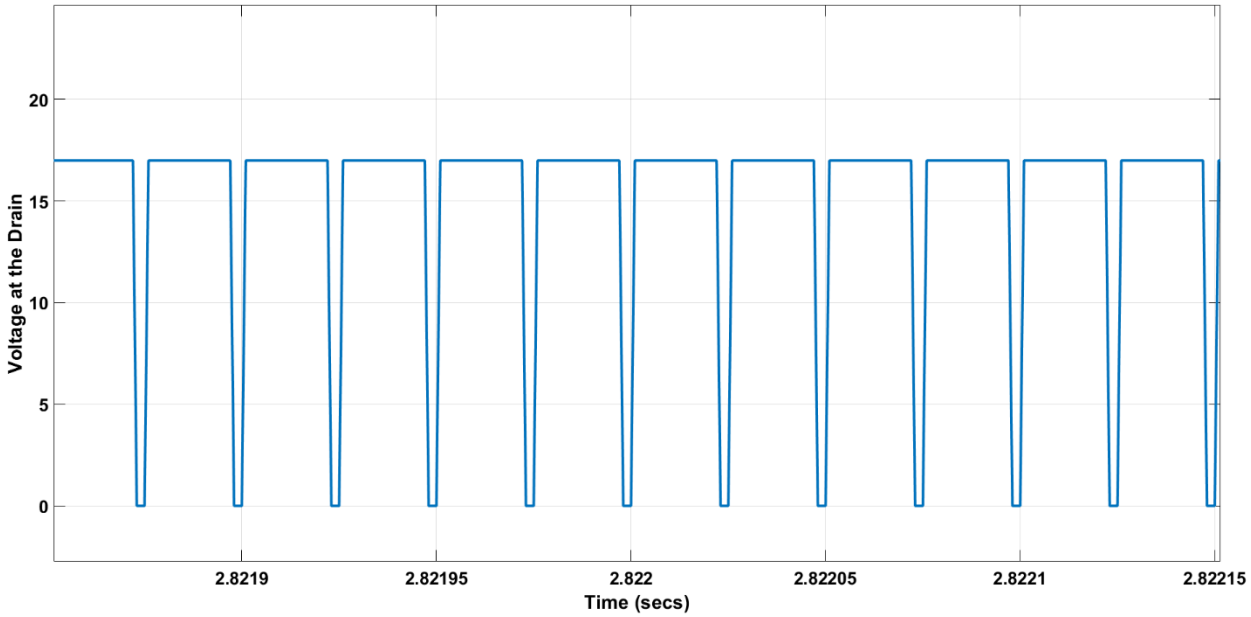

Figure 2.11: *MOSFET Drain to ground voltage when an input voltage of 17 V is switched with a PWM signal of frequency 40 kHz and duty cycle 87%.*

2.3.2.4 Diode

A diode is used in the buck converter to provide a return path during the switching off state.

2.3.2.5 LC Filter

The current and voltage supplied from the solar PV module has some ripple which may be harmful for the battery. Moreover, for enhancing battery lifetime, some standards need to be maintained (described briefly in the Engineering Standards section). Therefore, a LC filter is used in the buck converter to minimize the current and voltage ripple. This LC filter is a low pass filter which has a cutoff frequency much less than the switching frequency.

2.3.3 Feedback Circuit

As mentioned in the previous section, a constant battery voltage needs to be maintained at the battery terminal irrespective of the input voltage and circuit characteristics. Therefore, a feedback circuit serves the purpose of determining the correct duty cycle from the input voltage, output voltage and desired voltage at the battery terminals. The algorithm of the feedback circuit is shown below as a pseudo code. Then, a Simulink block is created to satisfy the algorithm (*Figure 2.12*).

Input:

V_{out} = Output voltage across the battery

V_d = Input voltage

V_{des} = the desired voltage at the Battery Terminal

Output:

D = Duty Cycle

Algorithm:

- Read the value of V_{out}, V_d and $V_{des.}$
- Found the Duty cycle given $D_{given}=V_{des}/V_{d.}$
- Calculate the duty cycle found Dfound=Vout/Vd.
- Calculate the error in duty cycle Derror=(Dgiven-Dfound)/Dgiven.
- Find out the duty cycle,D that should be given for making Vout=Vdes for the input voltage Vd (D=Dgiven/(1-Derror)).
- Instruct the Arduino to generate PWM of the calculated duty cycle (fixed frequency).

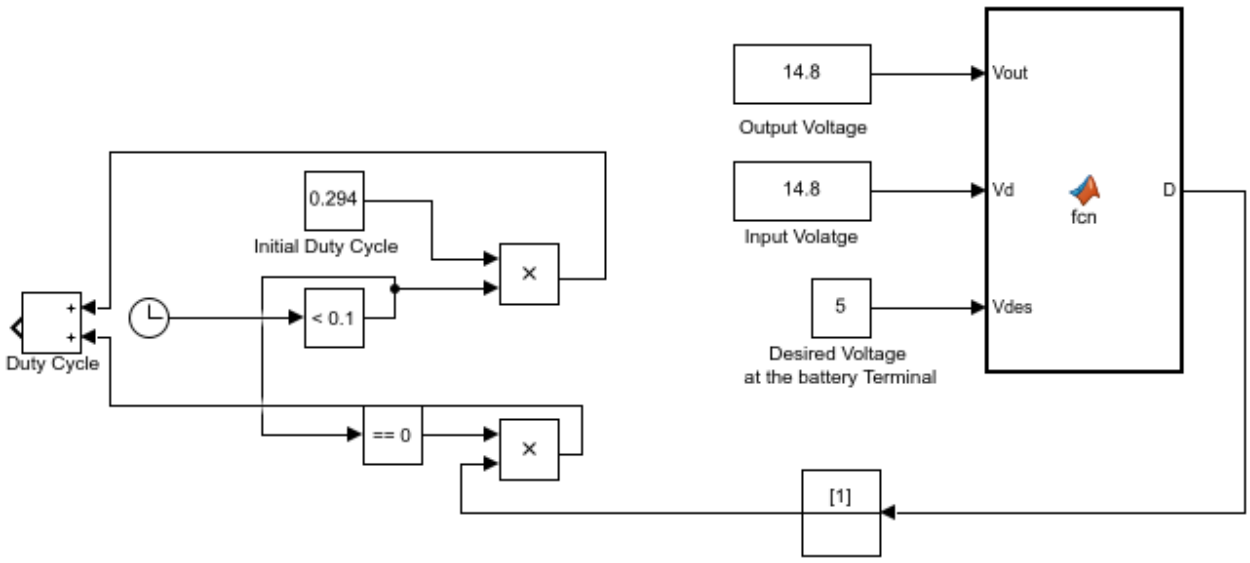

Figure 2.12: *Feedback circuit block diagram for the battery charging system in order to maintain constant voltage across the battery.*

2.3.4 MPPT

Maximum-power-point-tracking, or MPPT, can include one of several methods to obtain the maximum power from a solar PV module. In some cases, it may be possible to steer and direct a solar PV module so that it points directly towards the sun. This can have drastic effects on panel output power as the effective area of the solar panel is increased. In addition to tracking the sun through the sky, electrical load parameters may also be altered so that maximum power is extracted. *Figure 2.13* shows the current-voltage relationship of the KC85TS solar PV module.

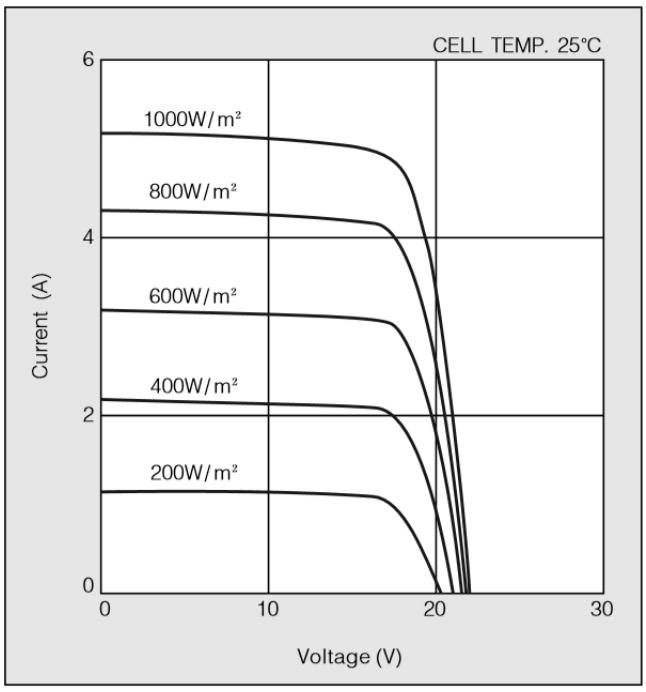

Figure 2.13: *I-V behavior of the Kyocera KC85TS (image reproduced from datasheet).*

Figure 2.14 shows a hypothetical current-voltage curve, below which is given a corresponding power-voltage curve. This demonstrates the relationship between solar PV module load and load power. If we are able to adjust the charging conditions of the battery (the load), we may be able to affect the power the battery is receiving. Increased power to the battery then implies increased charging rate.

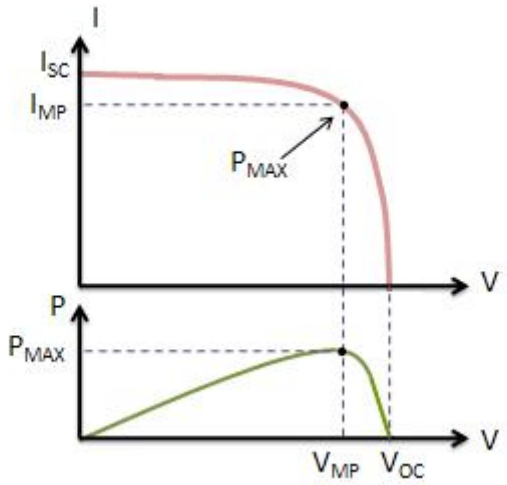

Figure 2.14: *Hypothetical solar PV current-voltage and power-voltage plots [3].*

Although accomplished in software, the MPPT algorithm is associated with a logical flowchart that may be considered an analog to a circuit schematic. *Figure 2.15* shows the perturb and observe algorithm flowchart. A circuit parameter, in this case V_{ref}, is changed slightly and the corresponding power change at some point in the circuit where maximum power is desired is observed. If the power increases, the same change to V_{ref} is made, and the process is reiterated. If the power decreases, the opposite change to V_{ref} is made, and the process is reiterated.

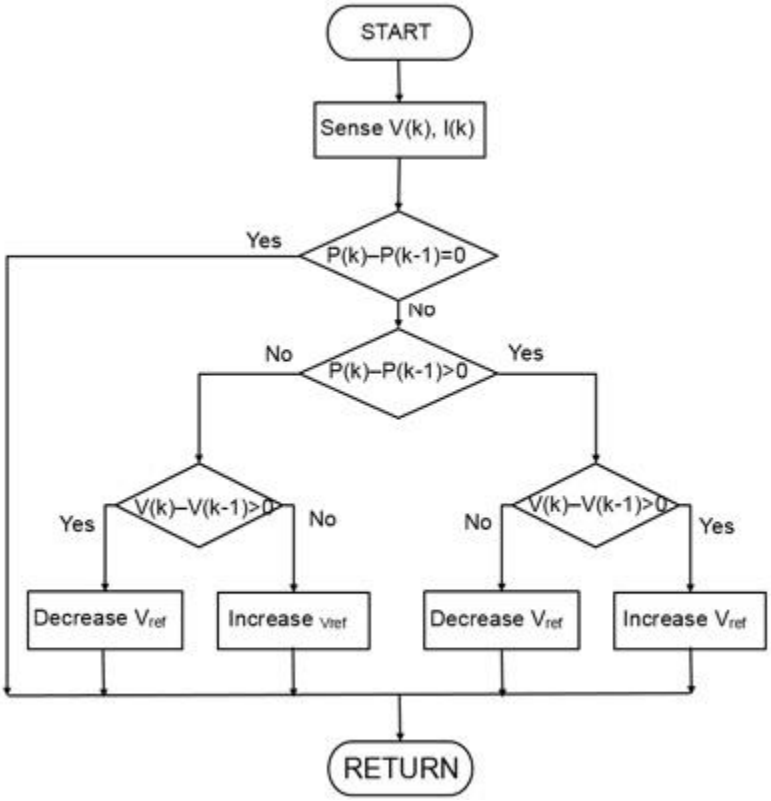

Figure 2.15: *MPPT perturb and observe algorithm flowchart [4].*

2.4. Engineering Standards

Engineering standards are some specification that should be met through the design. In this project, it is very important to maintain certain battery energy standards. In a battery charging system, the charge return factor (CRF) is a very important measure of the system's charging quality. CRF is the ratio of the amount of charge delivered to the battery during charging to the amount of charge delivered by the battery during discharge [5]. According to the California Energy Commission (CEC), the CRF should be less than 1.10 for 80% depth of discharge (DOD) and 1.15 for 40% DOD. It is not clear to me how to ensure this in our project. It is stated in the CEC standard that power efficiency should be greater than 89%. This is ensured in our project by

proper design of filters, switching circuits and compensating error amplifiers. Power factor in a battery charging system should also be maintained at greater than 90%.

The PV module being simulated is the KC85TS, which maintains UL1703 certification. It maintains standard I-V characteristics, and the I-V curve varies with irradiance. Moreover, in our design, there are protections against overcurrent according to National Electric Code (NEC) standards. We have used appropriate protective measures against overcurrent from short-circuiting. We have also implemented proper grounding of our load for safe operation. The electrical and electronics components used in the design are compliant with IEC standards. Should the design be implemented in hardware, an Arduino acting to provide control logic and functions would be programmed using the standard C++ programming language.

An additional standard that impacts this design is the Universal Serial Bus (USB) standard. Devices utilizing USB connections are numerous, and therefore, accommodating these devices in this design was desirable. USB standards set the nominal voltage requirement of this design to 5 V. To be more precise, the USB voltage standard is 4.4 to 5.25 V for low-power devices and 4.75 to 5.25 V (± 5%) for high power devices [6]. Thereby, battery charging standards helps to maintain good charging quality through CRF, PF and other parameters.

2.5. Critical Technological Challenges

In the development of power conversion system for solar battery chargers with maximum power point tracking, the following technological challenges arose:

To work with the Arduino, a challenge arises that will it be able to turn on the MOSFET to operate in its saturation region. The output of the Arduino is not sufficient to turn the MOSFET on. In overcoming the problem we used a gate drive circuit to amplify the current enough to turn on the MOSFET.

While implementing MPPT tracking technique, which is commonly used to maximize the output from the solar module, we found mismatch of duty cycles with the feedback circuit. In addition, it should not engage with the feedback circuit which serves to maintain the desired voltage at the battery terminal. Therefore, in order to maximize power from the solar module, we have regulated the desired voltage range from 14.8 V to 14.6 V and the feedback circuit will according change the output voltage and output current by changing the duty cycle. But, this method does not seem effective. Although, the power almost remains constant in this tiny input voltage variation, it was not efficient with significant amount of voltage change.

The perturb and observe algorithm has some own basic limitations due to its simplicity. It has two step size for increasing or decreasing voltage with referenced one. This method requires oscillating power output around the maximum power point even under steady state irradiance which will not suitable in rapid changing irradiance [7]. This leads to our mismatch in duty cycles with our designed feedback circuit. Increasing step size is a potential solution for this problem. However, this is just a conjecture based on internet resources. We yet need to implement it.

Another concern arises while using MOSFET as a switch, because it is very susceptible to overload voltages at the transition from turn on to turn off which can cause potential damage to the circuit. A snubbing circuit can be a way to dissipate the overload voltages. Because it provides an alternative way to bypass the current. We intend to use Schottky diode in circuitry to clamp the gate drain voltage of the MOSFET before COVID-19 case.

In doing this simulation based project, we did face several challenges and tried to overcome them through our knowledge and suggestion from our professor. Although we could devise some solutions associated with the specific problem, some cases we could not thrive.

2.6. Engineering Constraints (Trade-Offs)

The practical operation of the circuit is different from the ideal condition due to some engineering constraints. The output voltage from solar module varies depending on the light intensity it is exposed to throughout the day. On the contrary, the voltage across the battery terminal is to be kept constant. One way to overcome this problem is to change the control voltage with respect to the change in input voltage. In our project, a microcontroller will keep reading the value across the input and output voltage and accordingly change the control voltage to supply desired output voltage at the battery terminal.

In general practice, the control voltage for the PWM signal is the amplified signal of the error voltage. But when the control voltage is regulated by the error voltage, a slight mismatch in gain calculation can cause the control voltage falls below the desired duty cycle and we have faced this problem when designed type-2 and type-3 error compensator. Therefore, it is comparatively better to read the output voltage, input voltage from the circuit in the microcontroller and calculate the desired duty cycle in order to produce preferred output voltage.

A MOSFET needs minimum time (dead time) to charge the gate drive circuit which puts a limit on minimum on time and hence the output voltage. The output voltage and the duty cycle are also limited by the flattening of the sawtooth waveform from maximum to zero although ideally the time needed for this transition is zero. Moreover, a MOSFET has an operational range of 1 MHz but our buck converter operates around 40 kHz.

Because of all practical limitations discussed above and loss in the switch, inductance and capacitance, duty cycle in practical circuits is different from the ideal buck-converter's duty cycle. In this project, we have calculated the boundary value of the duty cycle considering those constraints (including varying input voltage). Considering the boundary value of the duty cycle, we will calculate minimum output voltage, maximum value of the critical inductance and minimum value of the capacitance to meet all design requirements. Moreover, every battery has its own resistance, inductance, capacitance and every capacitor and inductor has other parasitic RLC parameters. In our design, we have considered those values in order to find the optimum operating condition. In a summary, the performance of the buck converter is limited by the duty cycle performance of the MOSFET and the filter.

2.7. Societal Effects of Design

Any completion of prototyping (physical realization) that may occur on our part in the future will likely have a minimal effect on society and the environment. Much of the components used to complete the project could likely be reused in the future in the event of a teardown of the design. Other components not destined to be reused are minimal in weight, volume and value, and therefore their fate is largely irrelevant on a grand scale. Only minimal numbers of people would be aware of the prototype, and besides, the paradigm of solar PV utilization is already existent.

Beyond the practical discussion of the effects of completing a prototype, systems utilizing PV modules and their proliferation have had a pronounced and discernable effect on society. In general, energy harvest from off-the-grid sources can mean higher quality of lives for those disconnected or far away from larger power delivery networks. Of course, this can easily be seen in Alaska, as there are many remote areas that likely will never accommodate a large electrical system. Solar energy and systems that take advantage of it can also give individuals independence from utility companies that otherwise (perhaps necessarily) maintain a monopoly on energy supply. At this point in time, given the cost of materials and equipment, solar energy can be somewhat less expensive than traditional forms, although not significantly

so. As of yet, these systems do not provide free or unlimited energy, so effects are limited relative to total demand.

Besides its practical utilization, the PV battery charging system contributes its weight to the green energy movement. 'Green' energy is becoming a more prolific, feasible, justifiable, and accepted form of energy. It is beckoned by the nearing twilight of fossil fuels, and represents a forced and major societal change from the status quo that has existed for at least the last 100 years of global scale industrialization and modernization.

This design requires materials and components whose production potentially affects people and the environment. With the details of the exact processes involved left unspecified, most industrial products are produced at the expense of the environment, and potentially employees who must be exposed to toxic elements. At large scales, problems such as these can cause great regional and even global concerns. The largest single elements of this system are the PV module, and the batteries of significantly different chemistries. Large-scale utilization of these products should be vetted to assure acceptable environmental and health.

To summarize, the scale of this project is relatively small and it is not particularly novel, so we can conclude that it will have a minimal impact on society. On the other hand, we still recognize certain significant impacts on society and the environment that this project and many others of its kind do have.

3. PSpice/MATLAB Simulations

3.1. Complete System Simulation

Before the simulation of the whole system, individual parts were simulated. The PV module is an essential part of the design and the simulation result from the PV module was justified by the theoretical calculation of the single diode model of the Kyocera KC85TS. Then, a MOSFET is chosen based on the maximum voltage at the drain to source terminal. Furthermore, the MOSFET has also low turn on and turn off time.

In our design, the switching frequency of the PWM signal is 40 kHz which is well above the audible range (20-20000 Hz). In order to reduce the high frequency transients, a low pass LC filter is used along with the MOSFET. For CCM (continuous conduction mode) operation, current through the inductor is to be maintained positive. This requires calculating the inductance value (critical inductance value) and inductor having higher inductance than that ensures CCM operation. The formula for the critical inductance is given below:

$$L_{crit} = \frac{(1-D)\times R\times T_s}{2} \quad (2)$$

We have considered minimum duty cycle possible to calculate critical inductance. But this critical inductance value is not enough to maintain low current ripple through the battery. Therefore, the value of the inductance is finally chosen based on the ripple constraints.
Equation 3 depicts the relation between the inductance and the current ripple:

$$L = \frac{V_o \times (1-D) \times T_s}{\Delta I_L} \quad (3)$$

Figure 3.2 and *Figure 3.2* respectively show the required inductance value for maintaining certain amount of current ripple through the 5 V and 12 V Battery.

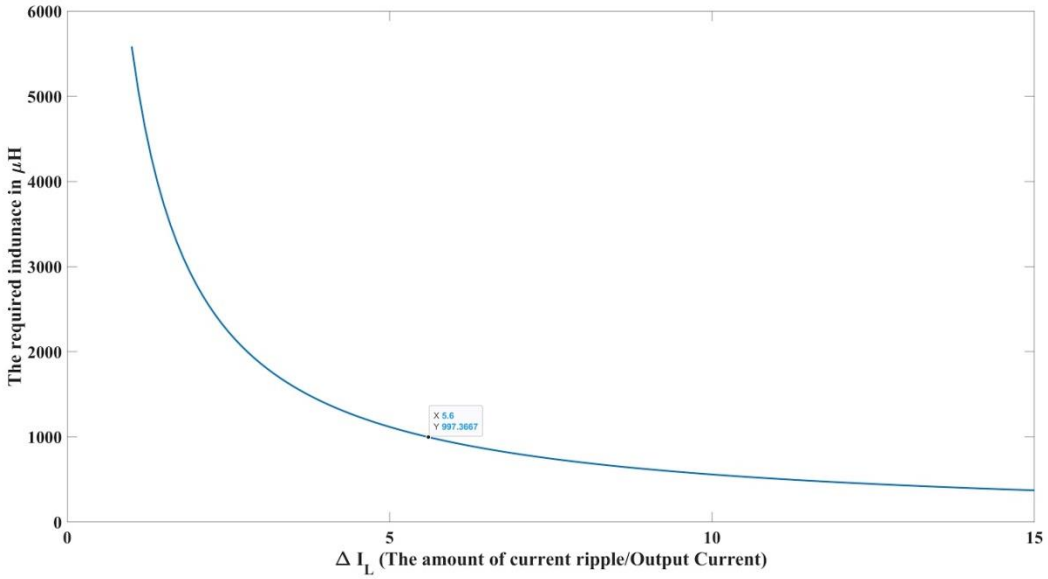

Figure 3.1: *Variation in current ripple with respect to inductance for the 5 V battery.*

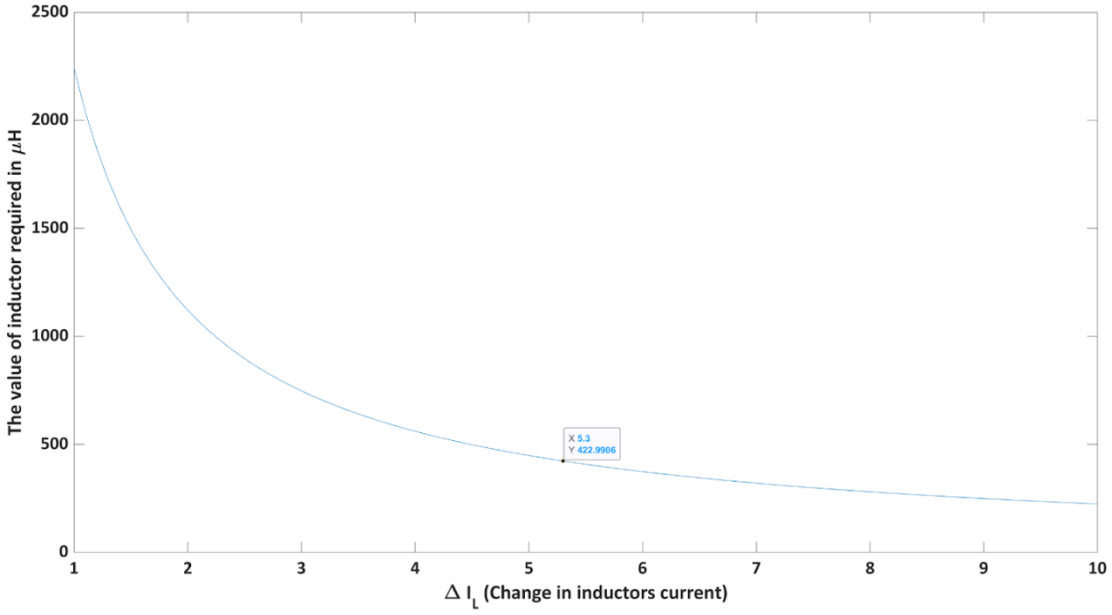

Figure 3.2: *Variation in current ripple with respect to inductance for the 12 V battery.*

Lastly, the parasitic resistance (r_c) of the capacitor is chosen by setting a constraint on the voltage ripple (equation 6) and capacitor is chosen based on this parasitic value.

$$r_c = \frac{\Delta V_o}{\Delta I_L} \tag{4}$$

The filtering specifications that have been used to simulate 12 V and 5V battery charger system are shown below:

<u>12 V Battery:</u>
Critical inductance, L_C = 11.21 µH
Inductor, L = 420 µH
Parasitic resistance of the inductor, r_L = 1.4 mΩ
Capacitor, C: 100 µF
Parasitic resistance of the capacitor, r_C = 0.0015 Ω
Cutoff frequency, fc = 776 Hz << 40 kHz

<u>5V Batery:</u>
Critical inductance, L_C = 55.85 µH
Inductor, L: 1000 µH
Parasitic resistance of the inductor, r_L = 2.1 mΩ

Capacitor, C: 100 µF
Parasitic resistance of the capacitor, r_C = 0.0015 Ω
Cutoff frequency, fc = 503 Hz << 40 kHz

Figure 3.3 shows the actual filter response of the 12 V buck converter. From the figure, it is apparent that the cutoff frequency (around 3.5 kHz) is slightly higher than what was calculated, since L, C has parasitic value which was not considered during calculation. But the cutoff frequency is lower than 40 kHz and the phase magnitude at this frequency is less than 180˚.

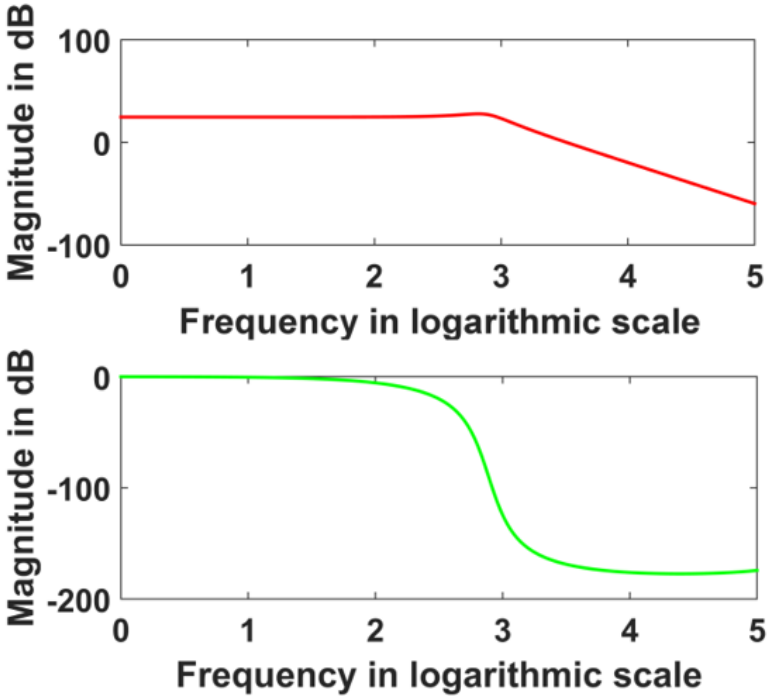

Figure 3.3: *Magnitude (top, frequency unit is hertz) and phase response (bottom, frequency unit is hertz) of LC filter for L: 420 µH, r_L = 1.4 mΩ, C = 100 µF, r_C = 0.0015 Ω, Fs = 40 kHz.*

Figure 3.4 and *Figure 3.5* show the complete charging system for the 5V and 12 V Battery respectively. In simulation, we have used resistor as a battery model since battery model of the Simulink did not provide us with the expected output. Probably, battery model may have been operated inappropriately. The powergui block shows the time step of every iteration which is much less than the time period of the PWM signal. Small time steps also help to meet the nyquist frequency criteria. The solar module is operated at the standard conditions (1000 W/m^2 irradiance and 25˚C temperature). The PV module, MOSFET and diode parameters are taken from the datasheet of the chosen components.

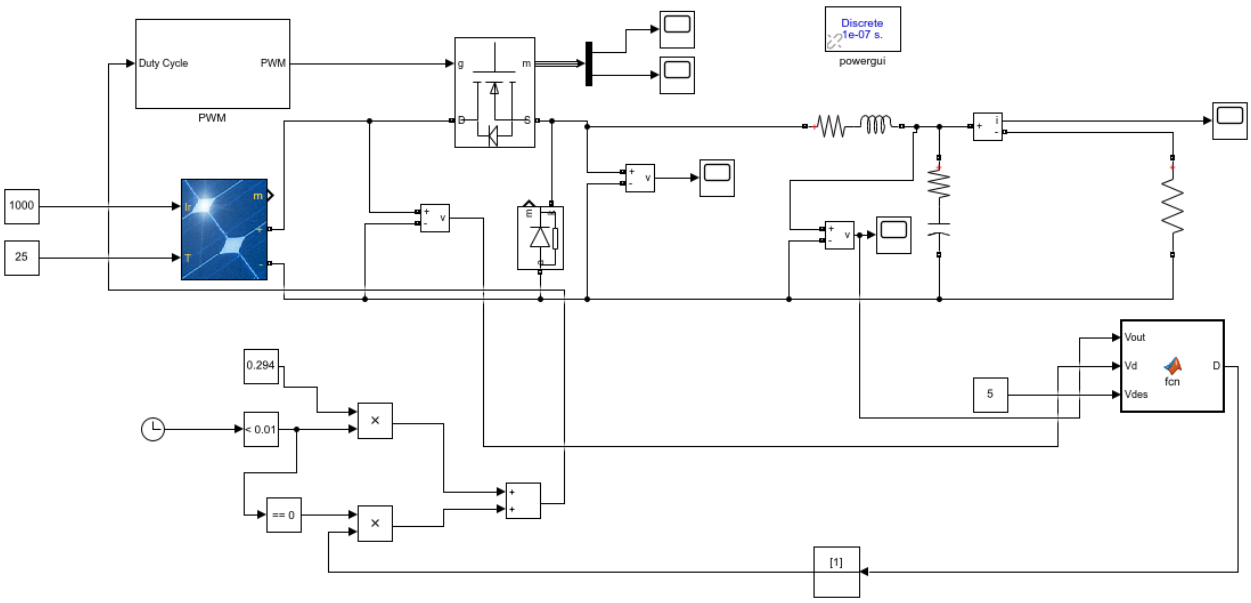

Figure 3.4: *12 V battery charging system from the solar module for the following specifications (L = 420 µH, r_L = 1.4 mΩ, C = 100 µF, r_C = 0.0015 Ω, Fs = 40 kHz, Kyocera KC85TS, Desired output voltage: 14.8 V).*

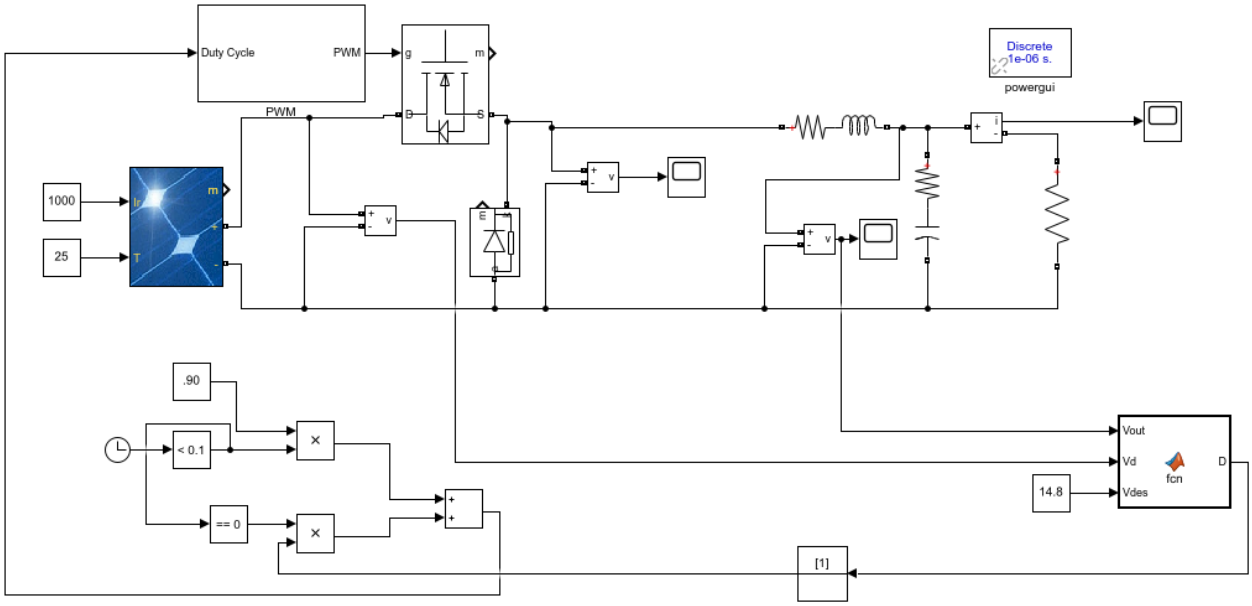

Figure 3.5: *5V V battery charging system from the solar module for the following specifications (L = 1000 µH, r_L = 2.1 mΩ, C = 100 µF, r_C = 0.0015 Ω, Fs = 40 kHz, Kyocera KC85TS, Desired voltage: 5 V).*

3.2. Gate Drive Circuit

We simulated, built and tested in hardware the basic, single-BJT gate drive circuit shown previously in *Figure 2.10*. The tests were conducted with circuit parameters that could accurately represent relevant conditions of the design. *Figure 3.6* shows the PSpice simulation

schematic and contains accompanying details within the simulation. The circuit utilizes a PN2222 BJT for signal amplification. The PN2222 was available throughout the semester in the UAF power electronics lab. This circuit in particular was chosen for its simplicity and adequacy. This circuit also did not impinge on the voltage potential difference from the solar PV module, which could in turn be fully applied to battery loads.

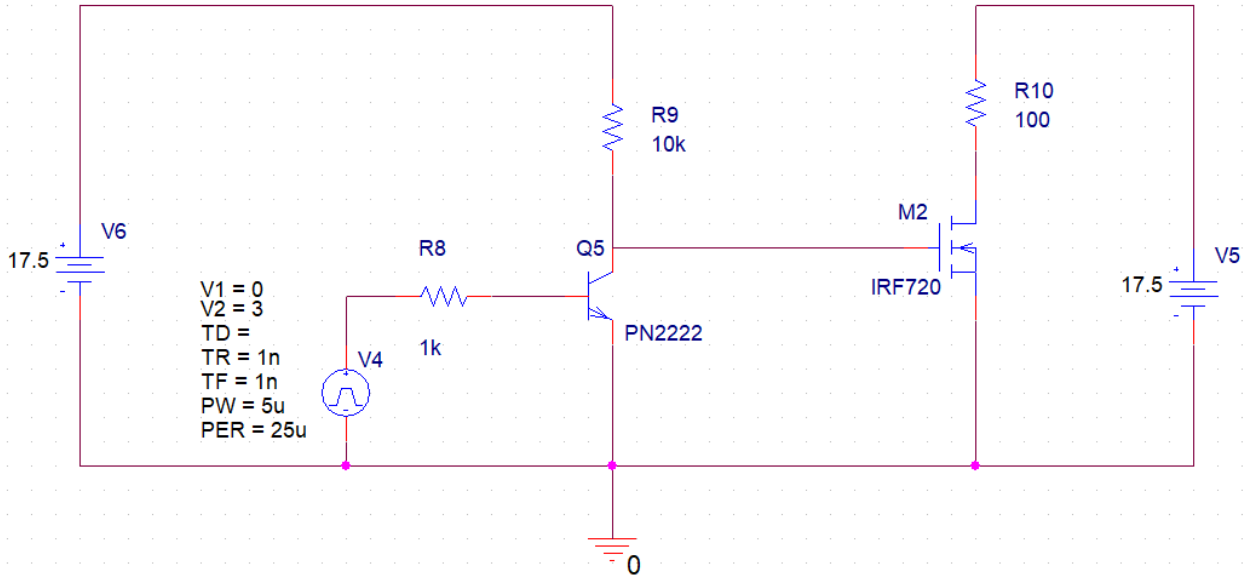

Figure 3.6*: *PSpice circuit schematic used for simulation of single-BJT gate drive circuit.

3.3. MPPT

Figure 3.7 shows our implementation of MPPT for our system. We used the perturb and observe algorithm to track our maximum power point. This is referred to as a hill climbing method, because it depends on the rise of the curve of power against voltage below the maximum power point. For the implementation, we used a 2 mH inductor and 1000 uF capacitor for our buck converter. The snubber resistance of the MOSFET was 3 Ω and the snubber capacitance was 143 pF. The output voltage of the system was around 15.6 V and current was around 5 A to charge the 12 V battery. We used a load resistance of 4.2 Ω. It is basically the battery internal resistance of .2 Ω and series connected resistance with value of 4 Ω [8]. The purpose of this circuit is to see whether we can extract maximum power from our solar PV module. The power of single solar module available in MATLAB® was about 76 watt. We did the experiment using irradiation settings of sunny day where the irradiation is generally increasing like a sine wave to peak value of 1100 W/m^2 [9]. The *Figure 3.8* shows the irradiation curve. Our MPPT max duty cycle value was set to 0.35 for bucking the voltage. Hence, we were able to get an average of 94% efficiency from MPPT. The efficiency measurement circuit is shown on *Figure 3.9*. Some further simulation can be done on

irradiation of intermittent cloud condition or rainy day where the irradiation is not increasing gradually.

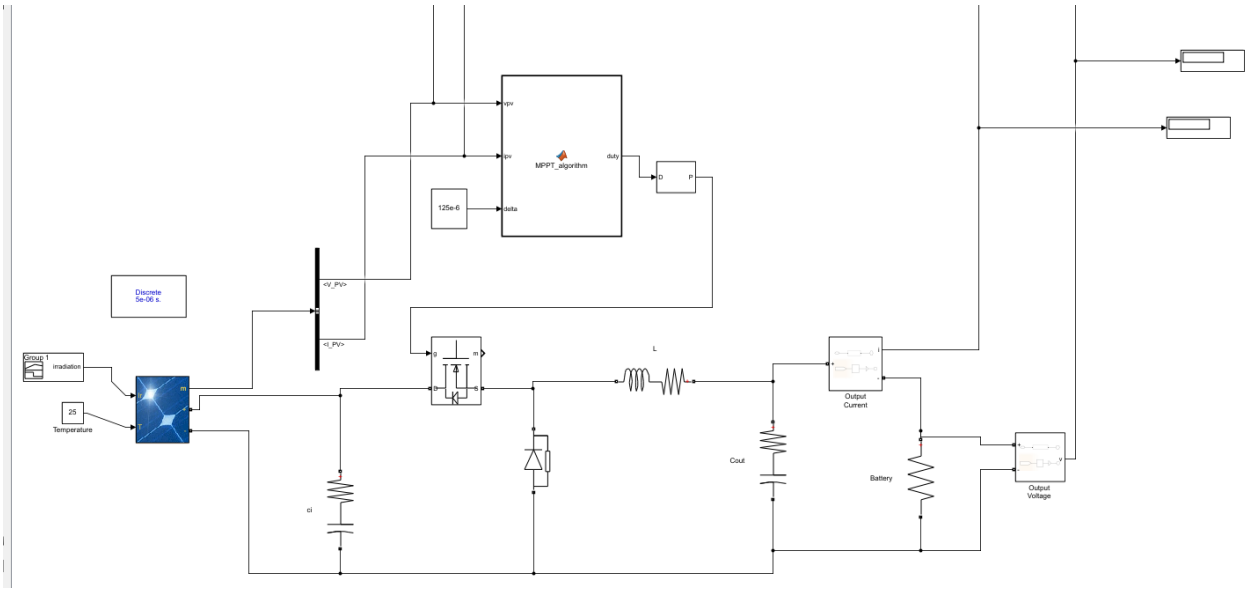

Figure 3.7: *Implementation of MPPT algorithm in our bucking circuit.*

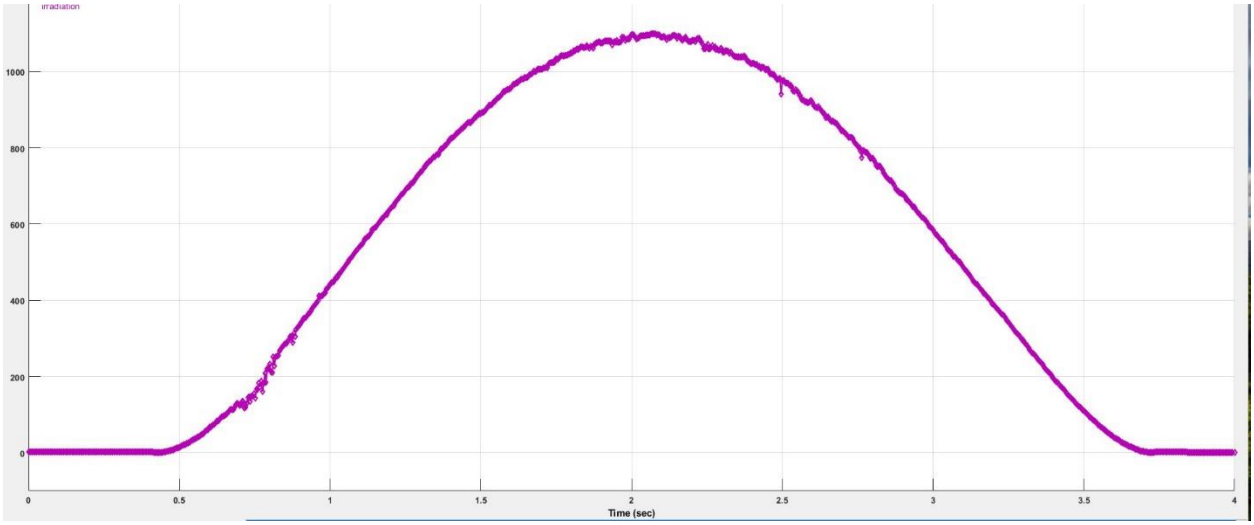

Figure 3.8: *Irradiation curve for checking MPPT with a Peak value of 1100 W/m^2.*

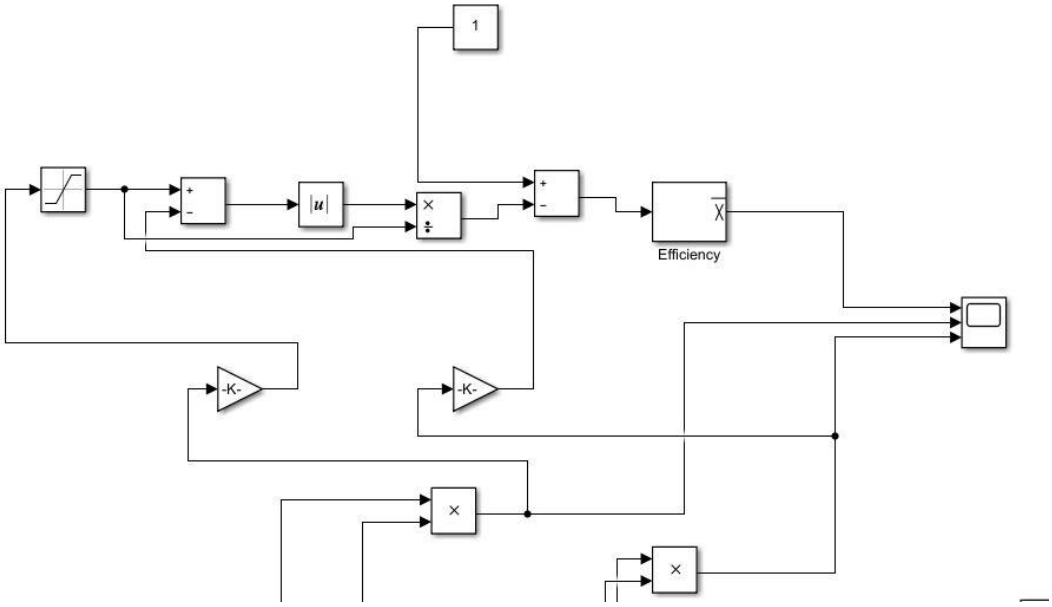

Figure 3.9: *The efficiency measuring circuit for MPPT.*

3.3.1 MPPT Tracking

We additionally simulated tracking of the MPPT within our 12 V battery subsystem. In one case, we used a 2.6 Ω resistor to approximate the load of a charging 12 V lead-acid battery of similar specification to that shown in Appendix B.2. We also increased the circuit load in order to demonstrate tracking. See Appendix C for an overview of the MATLAB® Simulink diagram used to conduct this simulation.

4. Simulation Test Results

4.1. 12 V Battery

The voltage and current across the 12 V battery terminals is shown in *Figure 4.1* and *Figure 4.2*. Unfortunately, when 14.8 V is set as the desired output voltage, around 14.6 V has been found across the battery terminals and therefore, the feedback circuit probably needs more sophistication. The battery charging current is found to be around 5.3 A which is expected. One more important thing is that the feedback circuit has been effective in reducing the transient in the voltage and current waveform.

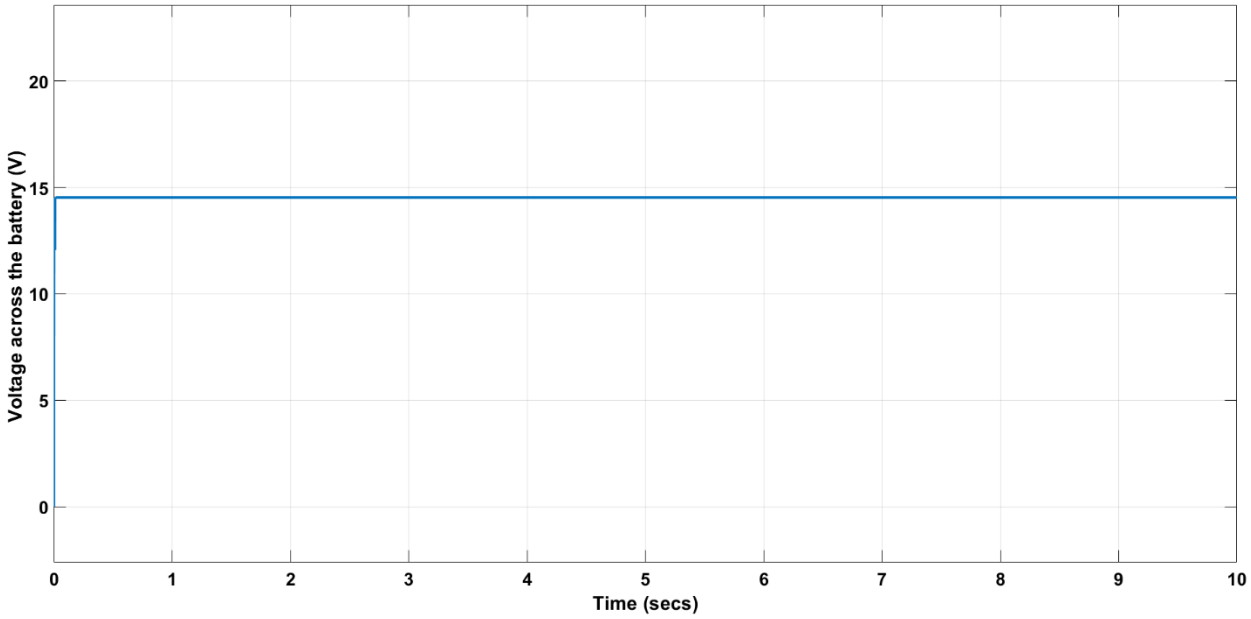

Figure 4.1: *Voltage across the 12 V battery terminals for the designed buck converter (L = 420 µH, r_L = 1.4 mΩ, C = 100 µF, r_C = 0.0015 Ω, Fs = 40 kHz, Kyocera KC85TS, Desired output voltage: 14.8 V).*

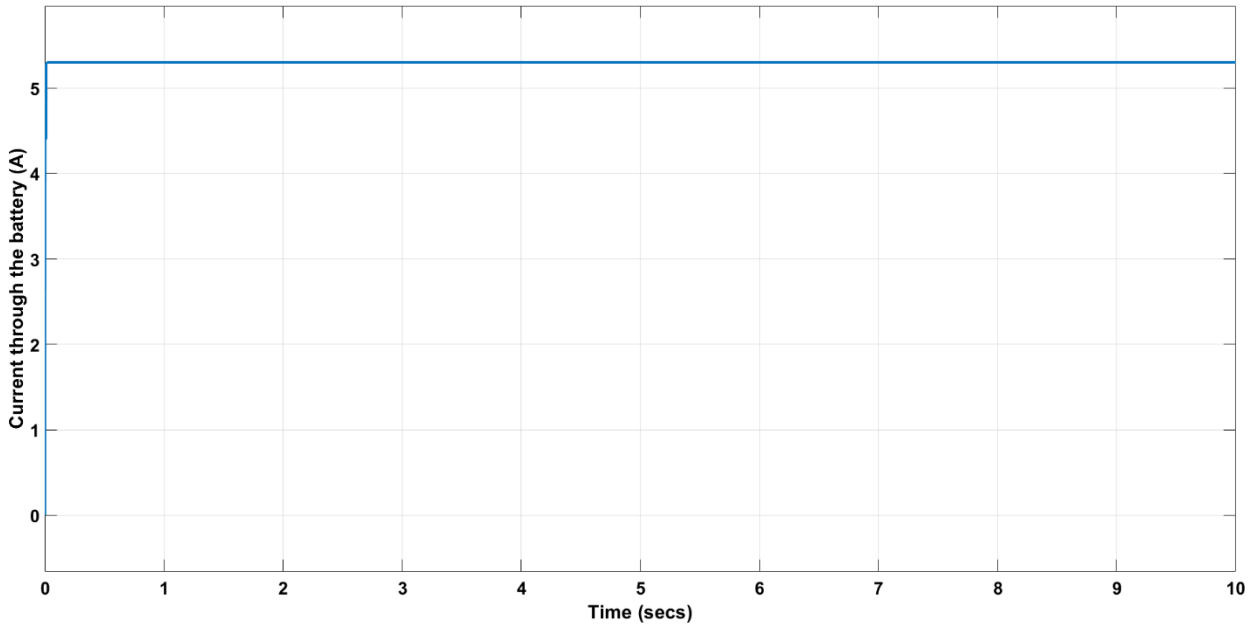

Figure 4.2: *Charging Current to the 12 V battery terminals for the designed buck converter (L: 420 µH, r_L=1.4 mΩ, C: 100 µF, r_C=0.0015 Ω, Fs=40 kHz, Kyocera KC85TS, Desired voltage: 14.8 V).*

We have done our calculation allowing less than 0.5% voltage ripple and around 5.2% current ripple in worst case condition. From *Figure 4.3* and *Figure 4.4*, it is clear that the voltage ripple is very small compared to 0.5% (around 5 mV) and the current ripple is almost negligible. This

result is not well understood although parasitic resistance of the inductor which has not been considered during the calculations may have made some impact. Later, we have altered our input voltage to observe our feedback circuits' performance. *Figure 4.5* shows that the output voltage is almost same when input has been changed from 17 V to 22 V. This proves the fact that the microcontroller based feedback circuit performs well for different input voltages.

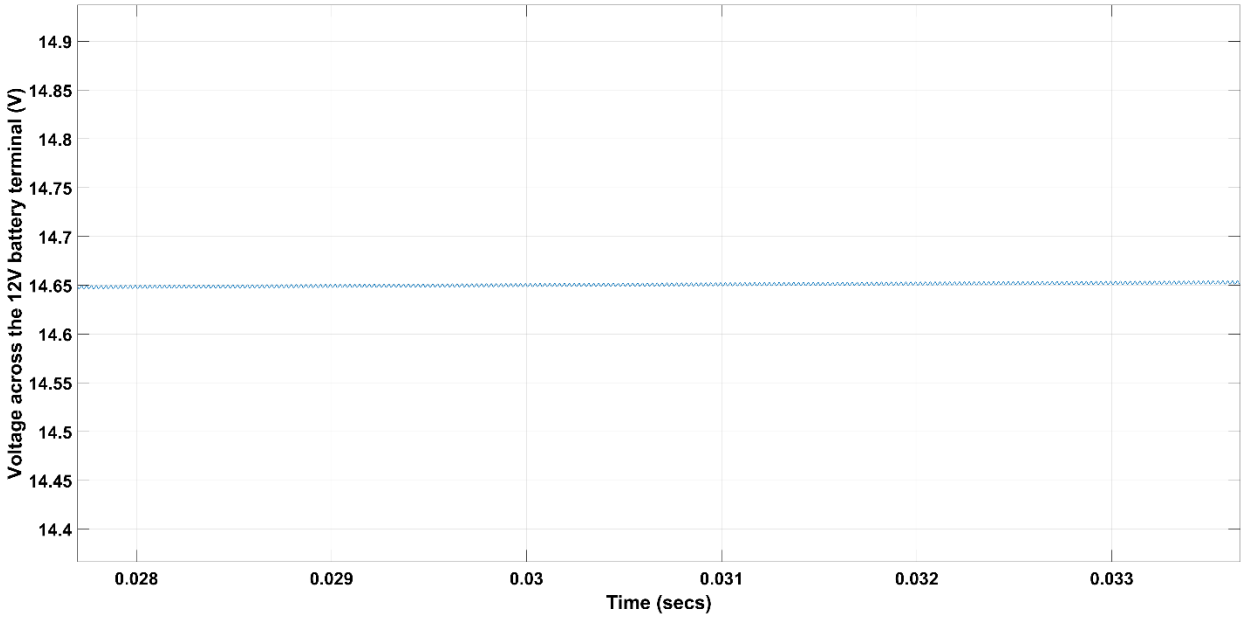

Figure 4.3: *Voltage ripple at the 12 V battery terminals for the designed buck converter(L = 420 µH, r_L = 1.4 mΩ, C = 100 µF, r_C = 0.0015 Ω, Fs = 40 kHz, Kyocera KC85TS, Desired output voltage: 14.8 V).*

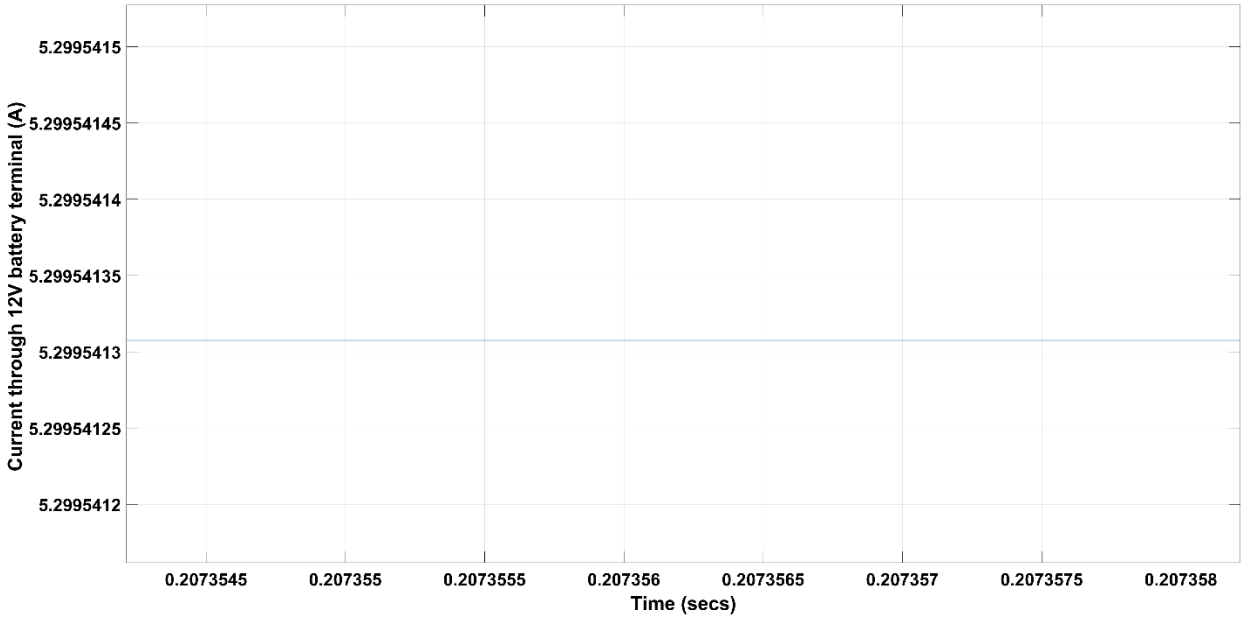

Figure 4.4: *Charging current ripple to the 12 V battery terminals for the designed buck converter (L = 420 µH, r_L = 1.4 mΩ, C = 100 µF, r_C = 0.0015 Ω, Fs = 40 kHz, Kyocera KC85TS, Desired output voltage: 14.8 V).*

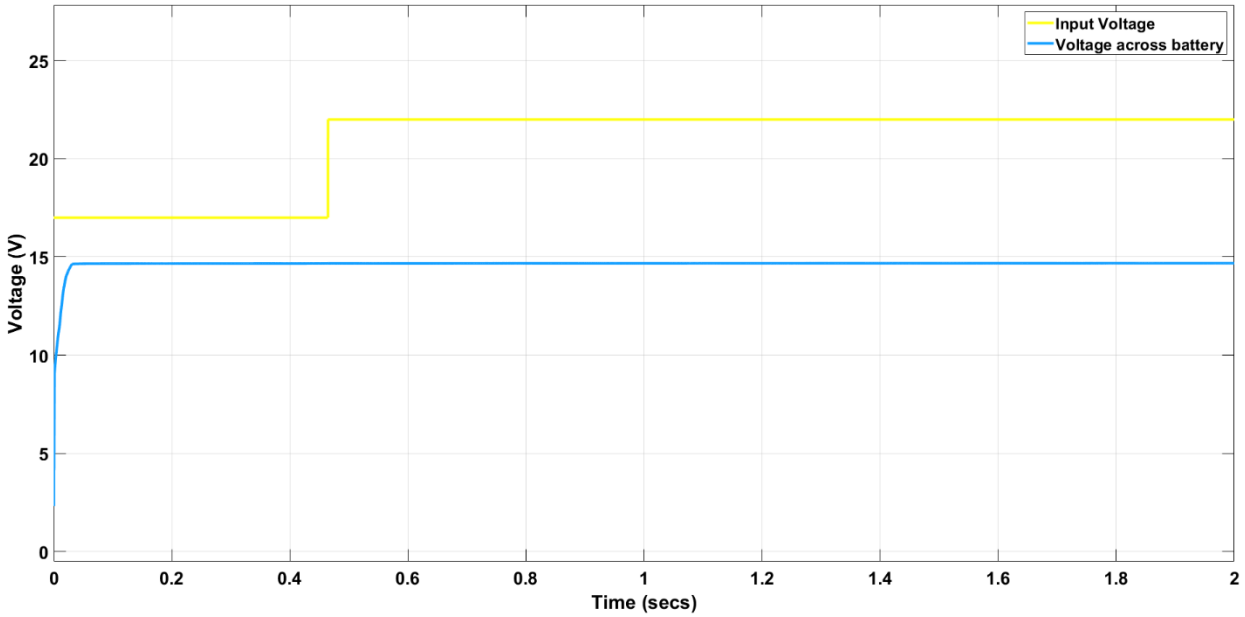

Figure 4.5: *Performance of the feedback circuit designed for the buck converter in order to maintain constant voltage across the battery terminals (blue).*

Figure 4.6 and *Figure 4.7* shows the voltage and current across the 5 V battery terminals. Battery terminal voltage is found to be almost 5 V which was set as the intended voltage and the battery charging current is close to 2 A. Therefore, 5V battery charging system is also effective in bucking voltage from the PV module. On the other hand, voltage and current ripple is much higher in the 5 V battery charging system than the 12 V battery charging system. From

Figure 4.8 and *Figure 4.9*, the voltage and the current ripple for the 5V battery is 0.18% and 0.9% respectively.

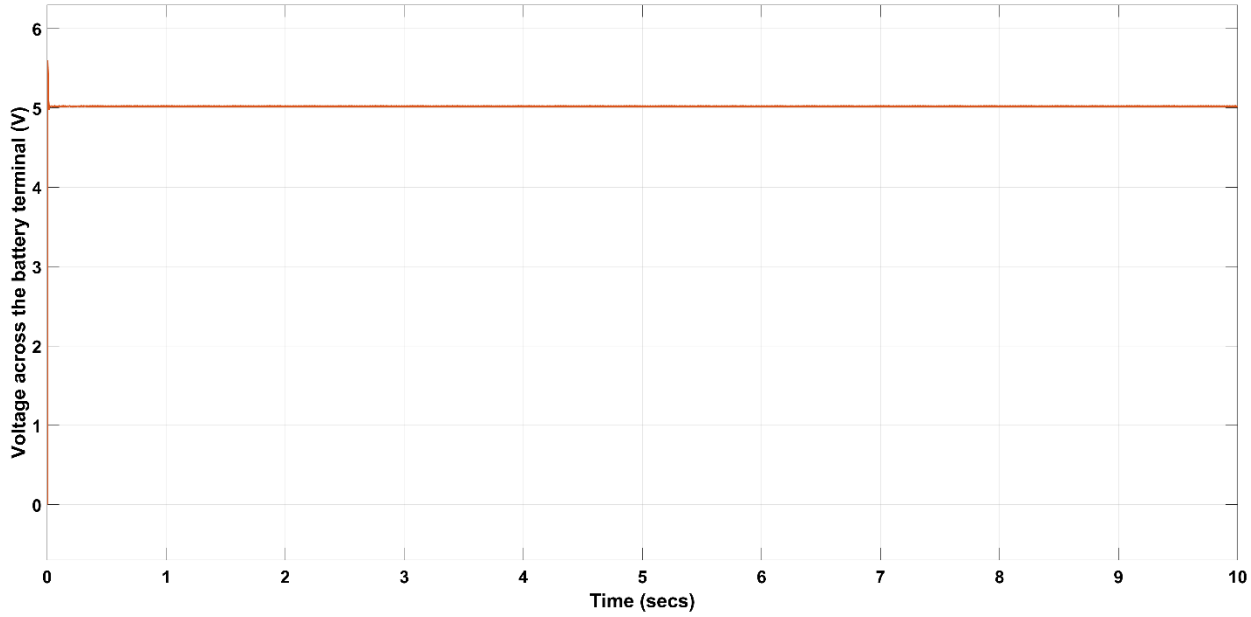

Figure 4.6: *5 V battery terminal voltage for the designed buck converter (L: 1000 µH, r_L=2.1 mΩ, C: 100 µF, r_C=0.0015 Ω, Fs=40 kHz, Kyocera KC85TS, Desired voltage: 5 V).*

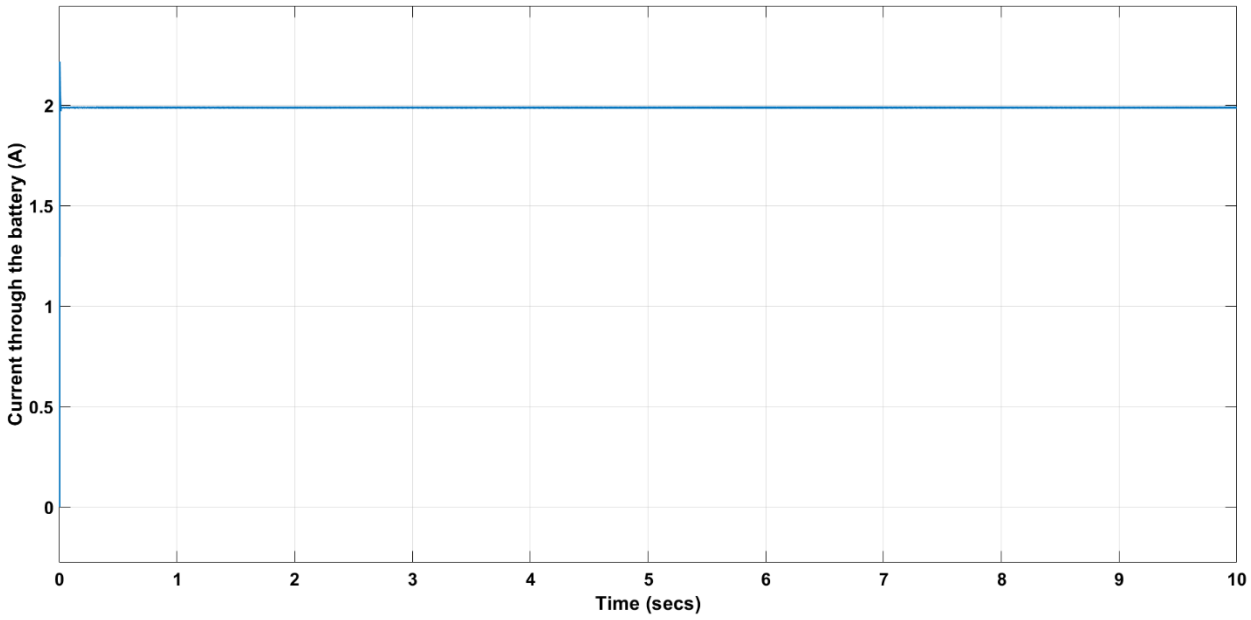

Figure 4.7: *5 V battery charging current for the designed buck converter (L = 1000 µH, r_L = 2.1 mΩ, C = 100 µF, r_C = 0.0015 Ω, Fs = 40 kHz, Kyocera KC85TS, Desired output voltage = 5 V).*

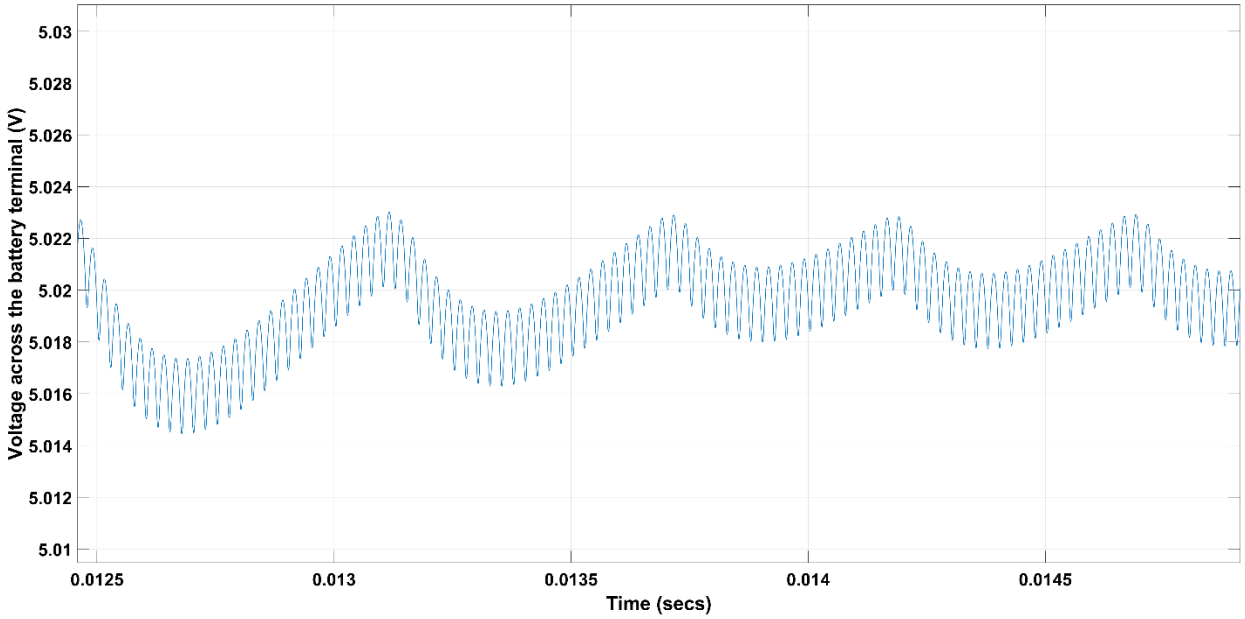

Figure 4.8: *5 V battery terminal voltage ripple for the designed buck converter (L = 1000 µH, r_L = 2.1 mΩ, C = 100 µF, r_C = 0.0015 Ω, Fs = 40 kHz, Kyocera KC85TS, Desired output voltage = 5 V).*

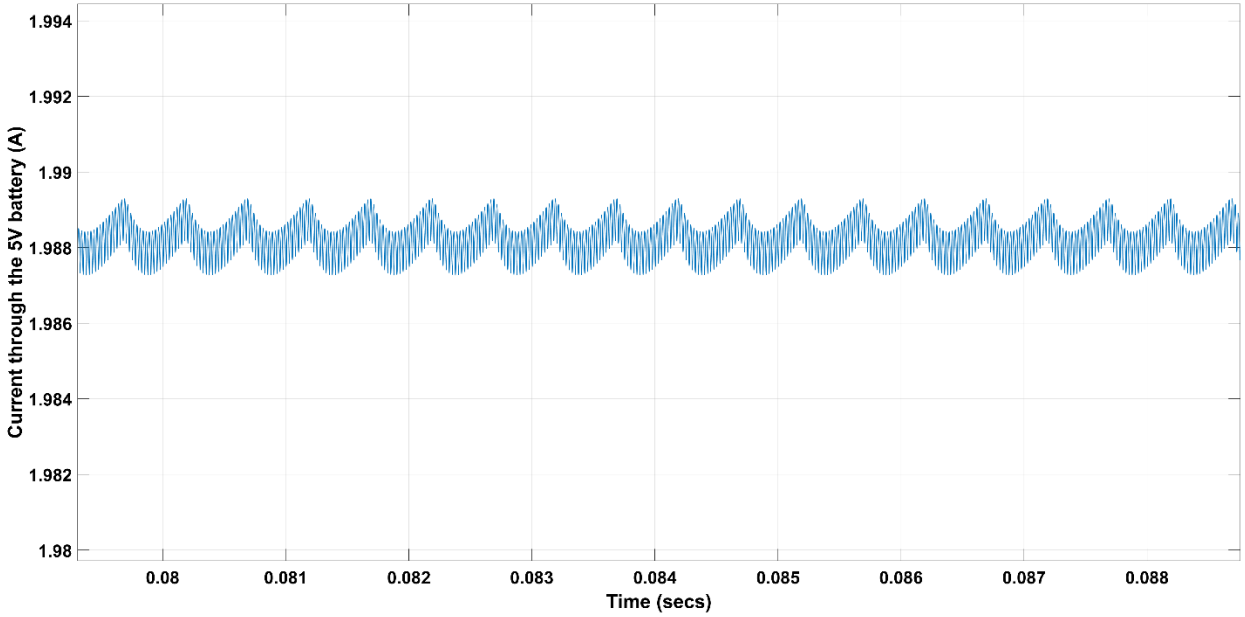

Figure 4.9: *5 V battery charging current ripple for the designed buck converter (L = 1000 µH, r_L = 2.1 mΩ, C = 100 µF, r_C = 0.0015 Ω, Fs = 40 kHz, Kyocera KC85TS, Desired output voltage = 5 V).*

4.2. Gate Drive Circuit

In simulating the gate drive circuit, we chose to use a signal duty cycle of 20 %. This signal later becomes inverted by the circuit. *Figure 4.10* and *Figure 4.11* show select results from the simulation. The first figure shows the base current of the BJT. It shows that the peak current demand is about 2.3 mA, which is well within the capabilities of the Arduino to produce. *Figure*

4.11 shows the rising of the gate-to-source voltage of the MOSFET that is due to the gate capacitance, and is accompanied by a large current demand. After the gate-to-source threshold voltage is reached, the MOSFET becomes fully turned-on. *Figure 4.12* through *Figure 4.14* shows similar results across a range of duty cycles that could be demanded by the system controller.

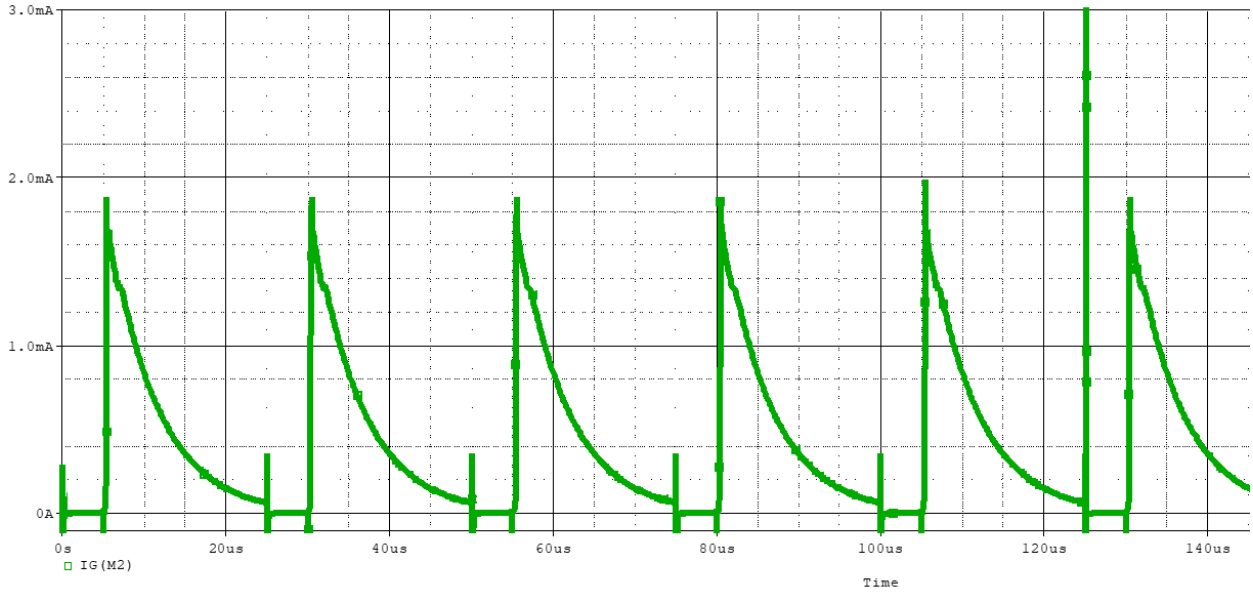

Figure 4.10: *Simulated base current requirements of the amplifying BJT in the single-BJT gate drive circuit (D = 20%).*

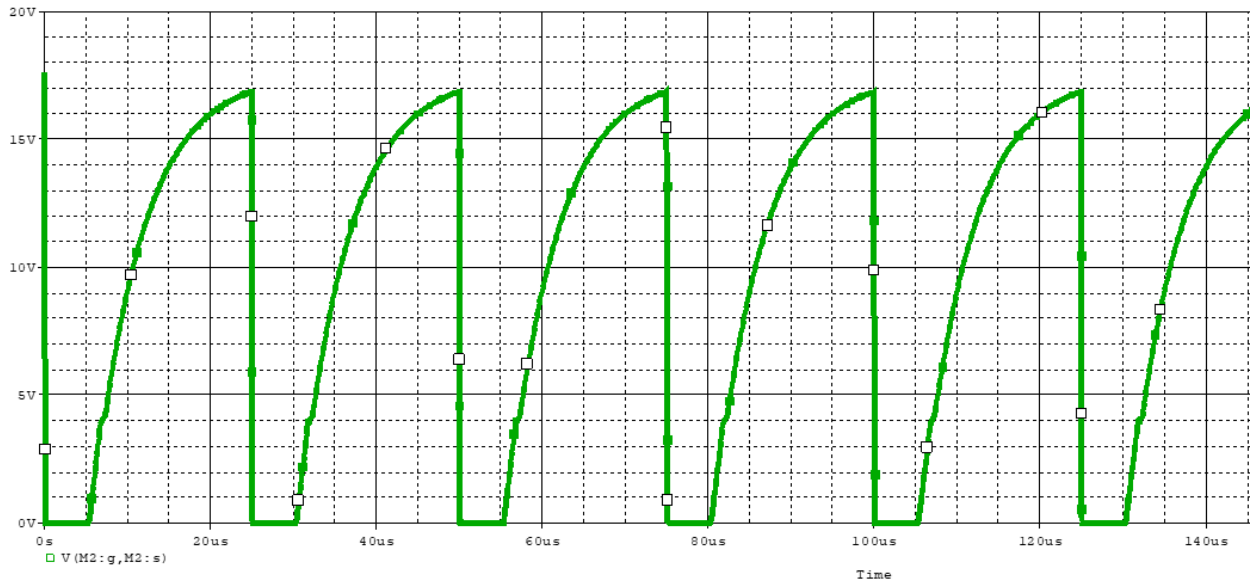

Figure 4.11: *Simulated gate to source voltage of the power MOSFET in the single-BJT gate drive circuit (D = 20%).*

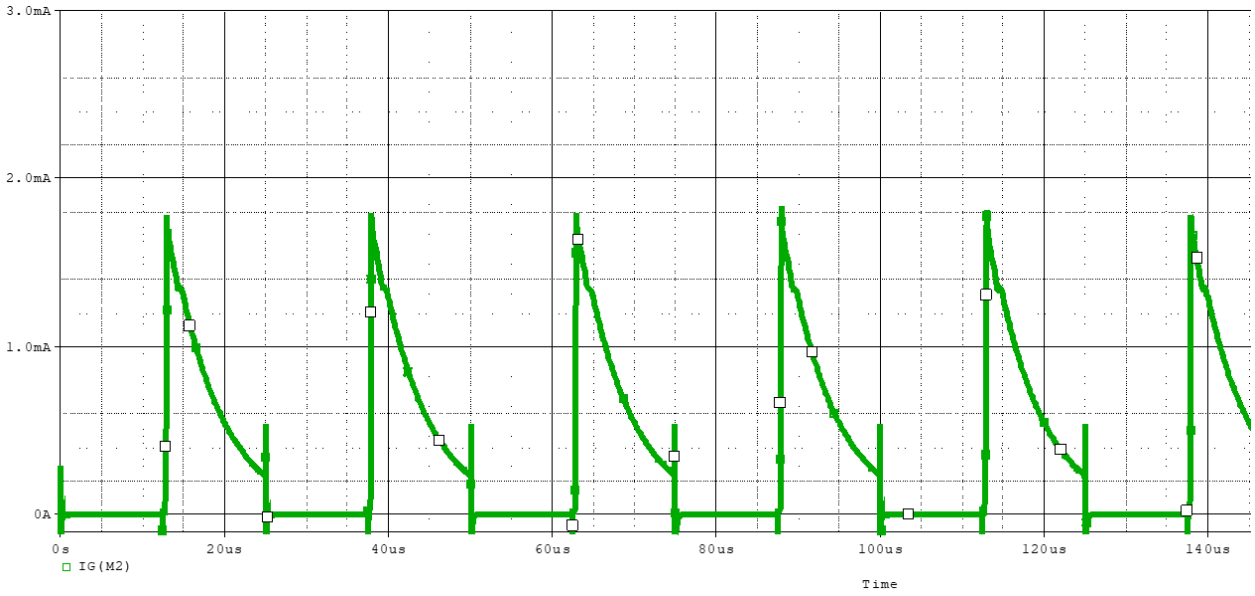

Figure 4.12: *Simulated base current requirements of the amplifying BJT in the single BJT gate drive circuit (D = 50%).*

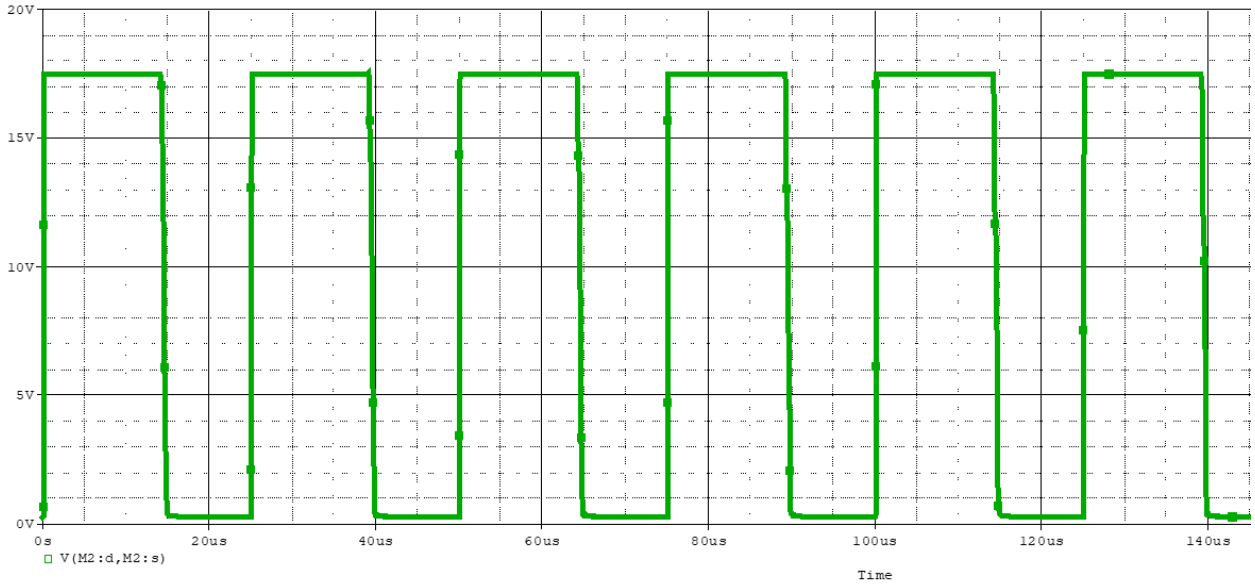

Figure 4.13: *Simulated drain to source voltage of the power MOSFET in the single BJT gate drive circuit (D = 50%).*

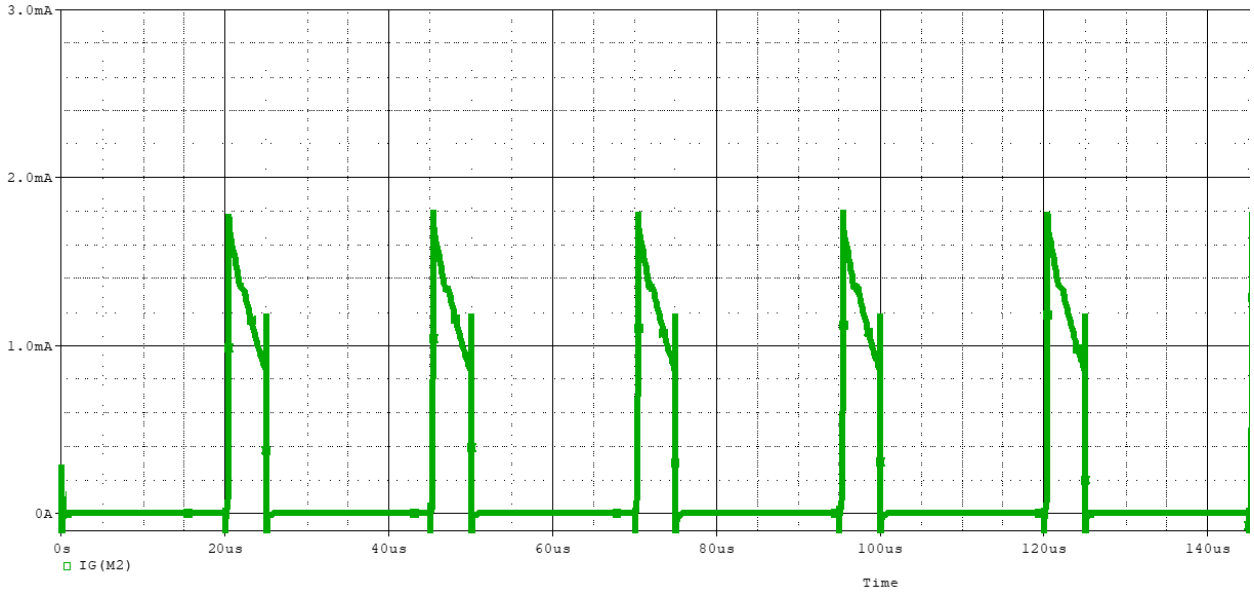

Figure 4.14: *Simulated base current requirements of the amplifying BJT in the single BJT gate drive circuit (D = 80%).*

Current requirements from the controller should remain at or below 2 mA, which is serviceable (up to 20 mA per Arduino GPIO pin: see Appendix B.3). *Figure 4.13* shows the MOSFET drain to source voltage (D = 50%), and indicates that the MOSFET is turning on correctly, with approximately an inverted duty cycle in comparison to the PWM signal being supplied to the BJT gate driver.

4.3. MPPT

Figure 4.15 is showing efficiency (blue), input power generated from the solar PV module (sky blue) and output power delivered to the load (red). Thus, from the comparison of input and output power the efficiency is calculated. The input power generated from the solar PV module was 76 watt whereas the output power was about 70 watt. The loss was due to parasitic resistance of inductor and capacitors and the ripple of the input current. From the curve we can see, efficiency is better when the power is starting to decrease (red dot on efficiency curve) for a certain amount of time.

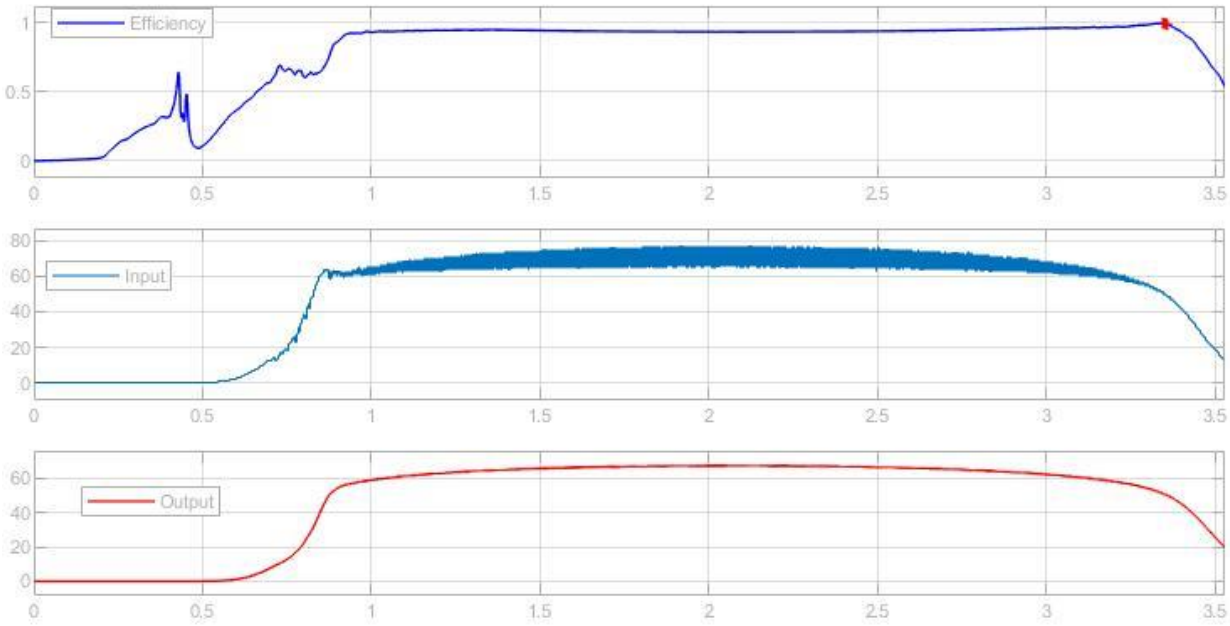

Figure 4.15: *Efficiency curve (blue), input power 76 watt (sky blue) and output power (70 watt) curve from MPPT feedback circuit.*

4.3.1 MPPT Tracking

Our tracking algorithm either applies the desired output voltage to a 12 V battery load, or outputs the maximum possible voltage if the solar PV module is not capable of suppling the full load. Should the Kyocera solar PV module be supplied with irradiation of 1000 W/m^2, it will be capable of supplying nearly its rated power to a 12 V battery (2.6 Ω resistor approximation). *Figure 4.16* shows circuit output power across the full range of switch duty cycles. *Figure 4.17* shows the corresponding output voltage; the peak voltage and peak power points coincide. From these figures we can also see that output voltage is not linearly related to switching duty cycle. *Figure 4.18* shows the tracking algorithm's behavior as it initiates loading from 0 V initial output under the same conditions. Seen in the figure, it achieves full output voltage at about 60 ms, and holds the voltage to within ± 0.05 V (12 V battery charging voltage is 14.6 V to 14.8 V). Algorithm response time is limited fundamentally by the analog circuit response time.

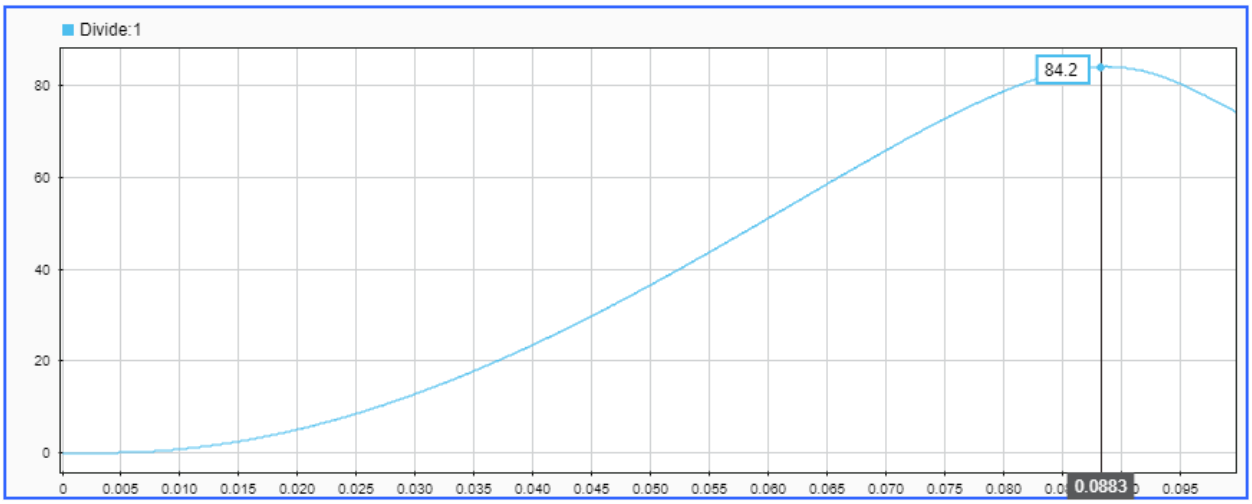

Figure 4.16: *Simulated 12 V charging circuit output power vs duty cycle with 1000 W/m^2 panel irradiance.*

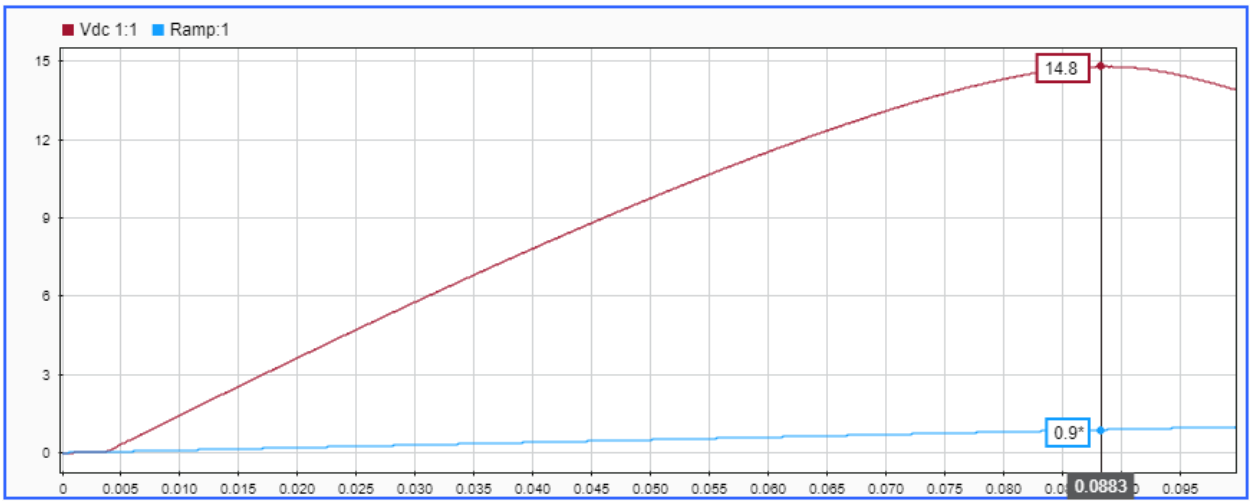

Figure 4.17: *Simulated 12 V charging circuit output voltage vs duty cycle with 1000 W/m^2 panel irradiance(red line is output voltage, blue line is switch duty cycle).*

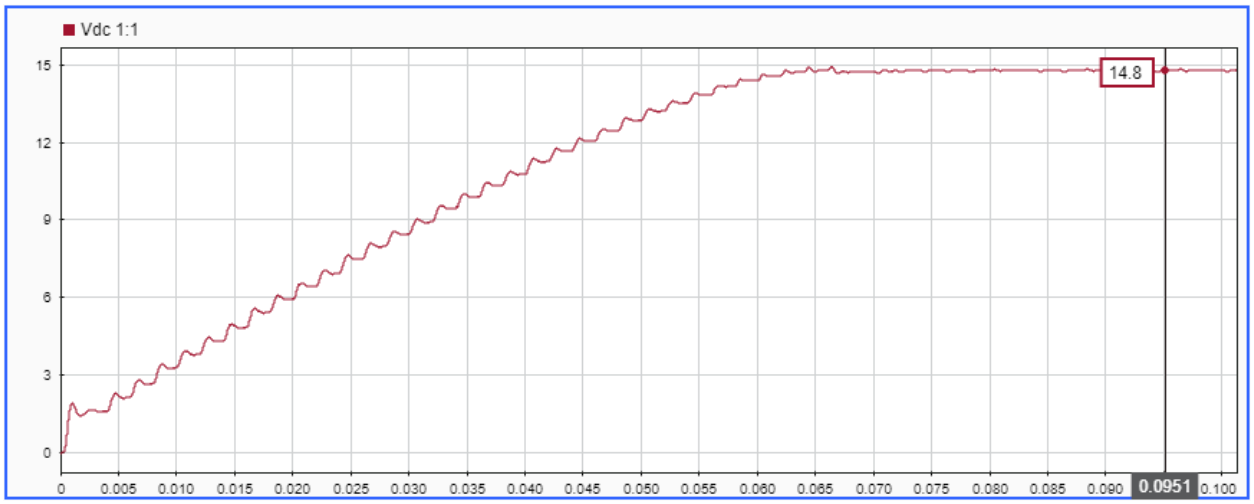

Figure 4.18: *Tracking algorithm response from 0 V to 12 V charging voltage target.*

As a further demonstration of the algorithm, we introduce a large load using a 0.5 Ω to the circuit. *Figure 4.19* shows the maximum output voltage and duty cycle with 1000 W/m^2 irradiance. *Figure 4.20* shows the circuit response to 500 W/m^2. A large reduction in output voltage (and power) is evident in both cases, and stronger nonlinear circuit response to input (duty cycle) is seen.

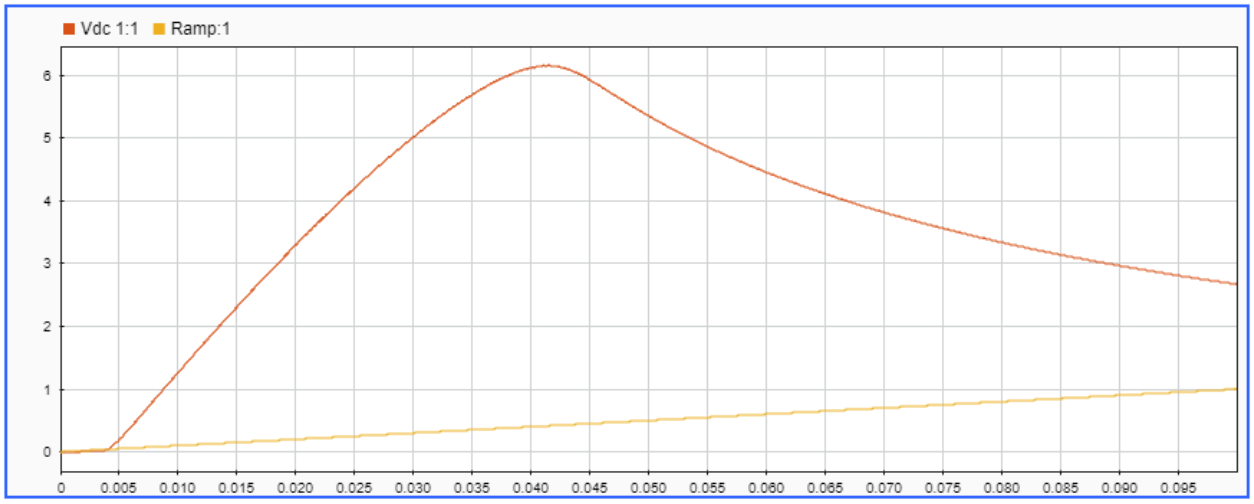

Figure 4.19: *High load 12 V charging circuit output voltage vs duty cycle with 1000 W/m^2 simulation irradiance setting.*

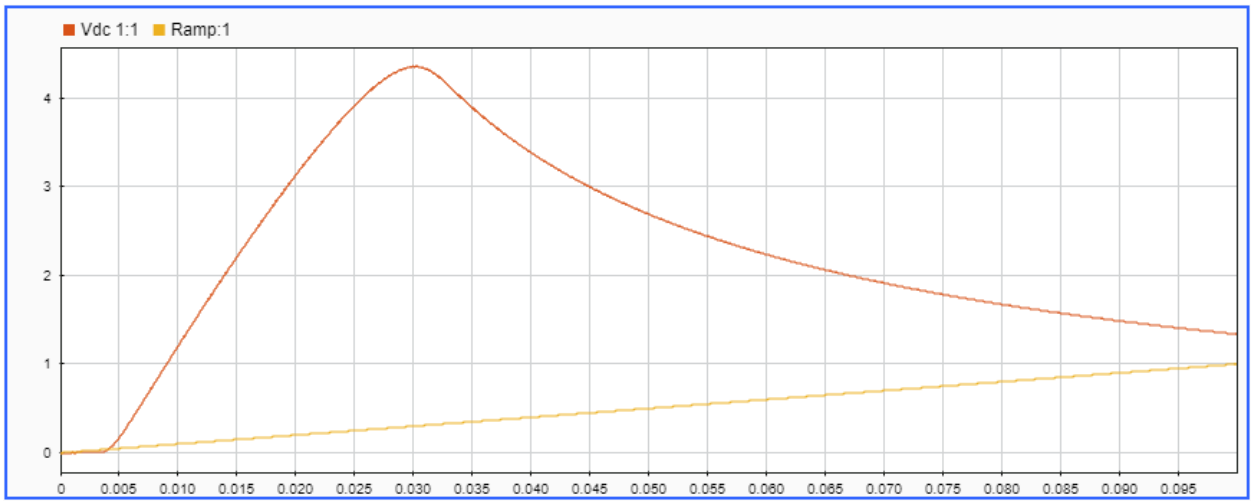

Figure 4.20: *High load 12 V charging circuit output voltage vs duty cycle with 500 W/m^2 simulation irradiance setting.*

Figure 4.21 demonstrates the tracking algorithm. In this case, the charging voltage of 14.6 V to 14.8 V cannot be achieved so the algorithm simply finds the maximum voltage. We altered the solar irradiance from 1000 W/m^2 to 500 W/m^2 simulation. At first, we can see the maximum possible voltage with 1000 W/m^2 reached at about 30 ms. The voltage is held until the irradiance drops, at which point the algorithm regains the (now lower) maximum possible output voltage within 30 ms of the reduction in system input power. A comparison between the figures shows the indeed, the point of maximum output is found.

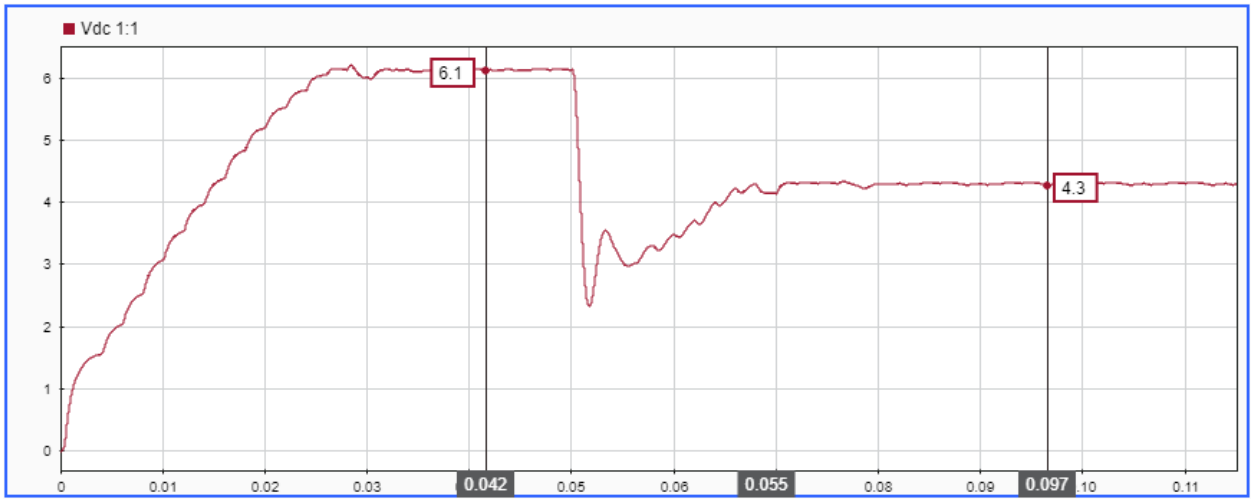

Figure 4.21: *MPPT tracking algorithm seeking and holding maximum possible output voltage under changing irradiance conditions.*

5. Final Component List and Budget

In this section, we will present suggested components that could be used to realize this design. Component pricing and a budget estimate are provided, along with some limited design rationales that justify the use of each component. Readers may find addition component data and specifications attached to this report as appendices.

5.1. Component List

First, refer to *Table 2* for a parts list. The table reflects the design to some extent as it is organized by circuit subsections.

Table 2: *Components List organized by circuit subsection with Part Numbers, Quantity and Cost.*

Component	Part Number	Quantity	Cost per Unit
System Power Source			
Kyocera 85W Solar Panel	KC85TS	1	$400.00
12 V Buck Converter			
power MOSFET	IPT60R065S7	1	$5.49
Schottky diode	RBQ20NS45ATL	1	$1.20
inductor (420 µH)	B82726E6333B040	1	$12.48
Capacitor (100 µF)	ST205C107MAN10	1	$45.11
MOSFET turn-off snubber resistor (3 Ω)	OD30GJE	1	$0.80
MOSFET turn-off snubber capacitor (143 pF)	MCM01-001ED(143)G-F	1	$4.25
5 V Buck Converter			
power MOSFET	IPT60R065S7	1	$5.49
Schottky diode	RBQ20NS45ATL	1	$1.20
Inductor (1000 µH)	B82726E6283B040	1	$12.48
Capacitor (100 µF)	ST205C107MAN10	1	$45.11
MOSFET turn-off snubber resistor (3 Ω)	OD30GJE	1	$0.80

MOSFET turn-off snubber capacitor (143 pF)	MCM01-001ED(143)G-F	1	$4.25
Gate Drive Circuits			
1 kΩ base resistor	OD102JE	2	$0.80
10 kΩ collector resistor	OD104JE	2	$0.80
gate drive BJT	PN2222	2	$0.24
Control Unit			
Arduino Uno Rev3	N.A.	1	$17.00
Pololu 7.5 V Step-Down Voltage Regulator	D24V22F7	1	$9.00
Additional Components			
12 Volt Lead-Acid Battery Load	UB12180	1	$35.00
USB Type A cable(s)	N.A.	(as needed)	$10.00
USB Type C cable(s)	N.A.	(as needed)	$10.00
electrical wire	N.A.	(as needed)	-

5.2. Budget

Continuing with the information from *Table 2*, a budget estimate was produced (*Table 3*).

Table 3: *Total system cost estimate with subsection subtotals.*

Subsection	**Cost**
System Power Source (PV Module)	$400.00
12 V Buck Converter	$69.33
5 V Buck Converter	$69.33
Gate Drive Circuits	$3.68
Control Unit	$26.00
Additional Components	$45.00
Final Budget Estimate:	$613.34

We believe that we used common and appropriate components in the design that provide a sufficient safety factor. If it was necessary to reduce the price of the system, we would first suggest a replacement capacitor for the buck converters. The capacitor included in the previous

tables provides excellent qualities, including a relatively low series resistance. Capacitors of the necessary parameters generally appear to be an expensive component, but our selection is particularly costly.

6. Workplan

As this project was conducted during the spring of 2020, project scheduling and progress was significantly impacted by the COVID-19 pandemic. Plans to create physical circuitry were cancelled, and validation of the design by simulation was focused on. This section contains a detailed description of the division of tasks among team members as was originally planned. Our working project Gantt charts are presented, and accurately represent our progress through the project before the U.S. response to COVID-19 took place. These charts provided scheduling constraints that facilitated timely project completion.

6.1. Division of Tasks

Tushar was selected to be responsible for any feedback and control circuitry incorporated into the design. He was responsible for any signal conditioning necessary to collect voltage measurements from the circuit and feed them to the microcontroller. Circuit measurements were to be taken from the solar PV module power source, the DC-DC converter outputs, and the batteries in an open circuit state or approximation thereof. This component of the project did not take place with no physical circuit created or operated. Tushar would also have been responsible for conditioning the signal outputs of the microcontroller. They must be conditioned and delivered as appropriate to the circuit, or very specifically, to the switching power MOSFETS.

Avro was responsible for the operation of the Arduino microcontroller. In our design, the microcontroller is singly responsible for determining the set points and functional behavior of the system. The control unit must be programmed to process the inputs it receives, and return appropriate outputs. Code that would have been implemented in the Arduino was instead implemented in MATLAB for purposes of the simulation. Code that Avro would have developed would deliver steady output voltages to the batteries despite a potentially variable input power supply. Avro was also tasked with incorporating an MPPT algorithm into the control scheme so that close to maximum charging current is safely delivered to the batteries. The microcontroller logic would also monitor battery status and adjust battery input as is necessary in an actual implementation of the design.

Nick was assigned to the power processing circuitry in the design, with DC-DC conversion concisely encompassing power conversion. In this case, there are a sequence of two separate buck converters that respectively feed the 12 V and 5 V batteries. The design of these converters emphasizes the Continuous-Current Mode (CCM) of operation, and includes parameters that maintain voltage output ripple to within acceptable and standard limits. The design of these circuits accommodate a full range of operating conditions, including potentially large transient currents and voltages.

6.2. Project Schedule with Gantt Chart

Refer to the subsequent attached pages to view the working project Gantt chart. These charts are valid prior to the social distancing restrictions put in place due to COVID-19 in March 2020. The chart includes the (assigned) tasks as outlined within the course Blackboard page. Deliverables, which are largely contained in the 'Management' section of the chart, are coincident and consistent with the EE608 spring 2020 course schedule (*Figure 6.1* and *Figure 6.2*). The more subjective scheduling in the 'Design' and 'Construction and Testing' sections was created with the intention to reflect a somewhat realistic semester long project progression, as well as maintain an identifiable sequence of task dependencies. *Figure 6.3* shows the design related work schedule, and *Figure 6.4* shows the intended scheduling prior to COVID-19 for the construction and testing project stages. Certain other considerations of scheduled events secondary to the project (such as the midterm and lab assignments) were also taken into consideration. Task division in the charts remained generalized, with each team member responsible for maintaining their own scheduling to accomplish their task in accordance with the Gantt charts.

WBS	TASK	LEAD	START	END	DAYS	% DONE
1	**Management**					
1.1	Reports					
1.1.1	Choose Teams	Team	Fri 1/17/20	Tue 1/21/20	5	100%
1.1.2	First Meeting / Choose Project	Team	Wed 1/22/20	Wed 1/22/20	1	100%
1.1.3	Work Plan	Nick	Wed 1/22/20	Thu 1/23/20	2	100%
1.1.4	Weekly Progress Report 1	Nick	Mon 1/20/20	Fri 1/24/20	5	100%
1.1.5	Weekly Progress Report 2	Avro	Mon 1/27/20	Fri 1/31/20	5	100%
1.1.6	Proposal	Team	Sat 1/25/20	Mon 2/03/20	10	100%
1.1.7	Weekly Progress Report 3	Tushar	Mon 2/03/20	Fri 2/07/20	5	100%
1.1.8	Weekly Progress Report 4	Nick	Mon 2/10/20	Fri 2/14/20	5	100%
1.1.9	Weekly Progress Report 5	Avro	Mon 2/17/20	Fri 2/21/20	5	100%
1.1.10	Weekly Progress Report 6	Tushar	Mon 2/24/20	Fri 2/28/20	5	100%
1.1.11	Midterm Progress Report	Team	Sat 2/22/20	Mon 3/02/20	10	75%
1.1.12	Weekly Progress Report 7	Nick	Mon 3/02/20	Fri 3/06/20	5	0%
1.1.13	Weekly Progress Report 8	Avro	Mon 3/16/20	Fri 3/20/20	5	0%
1.1.14	Weekly Progress Report 9	Tushar	Mon 3/23/20	Fri 3/27/20	5	0%
1.1.15	Weekly Progress Report 10	Nick	Mon 3/30/20	Fri 4/03/20	5	0%
1.1.16	Weekly Progress Report 11	Avro	Mon 4/06/20	Fri 4/10/20	5	0%
1.1.17	Draft Final Report	Team	Sat 4/04/20	Mon 4/13/20	10	0%
1.1.18	Weekly Progress Report 12	Tushar	Mon 4/20/20	Fri 4/24/20	5	0%
1.1.19	Final Report	Team	Sat 4/18/20	Wed 4/29/20	12	0%
1.2	Presentations					
1.2.1	Proposal	Team	Sat 1/25/20	Mon 2/03/20	10	100%
1.2.2	Midterm	Team	Sat 2/22/20	Mon 3/02/20	10	75%
1.2.3	Demonstration	Team	Sat 4/18/20	Mon 4/27/20	9	0%
1.2.4	Final	Team	Sat 4/18/20	Wed 4/29/20	12	0%

Figure 6.1: *Gantt chart of managerial tasks for weeks 1-7 (week 8 is void).*

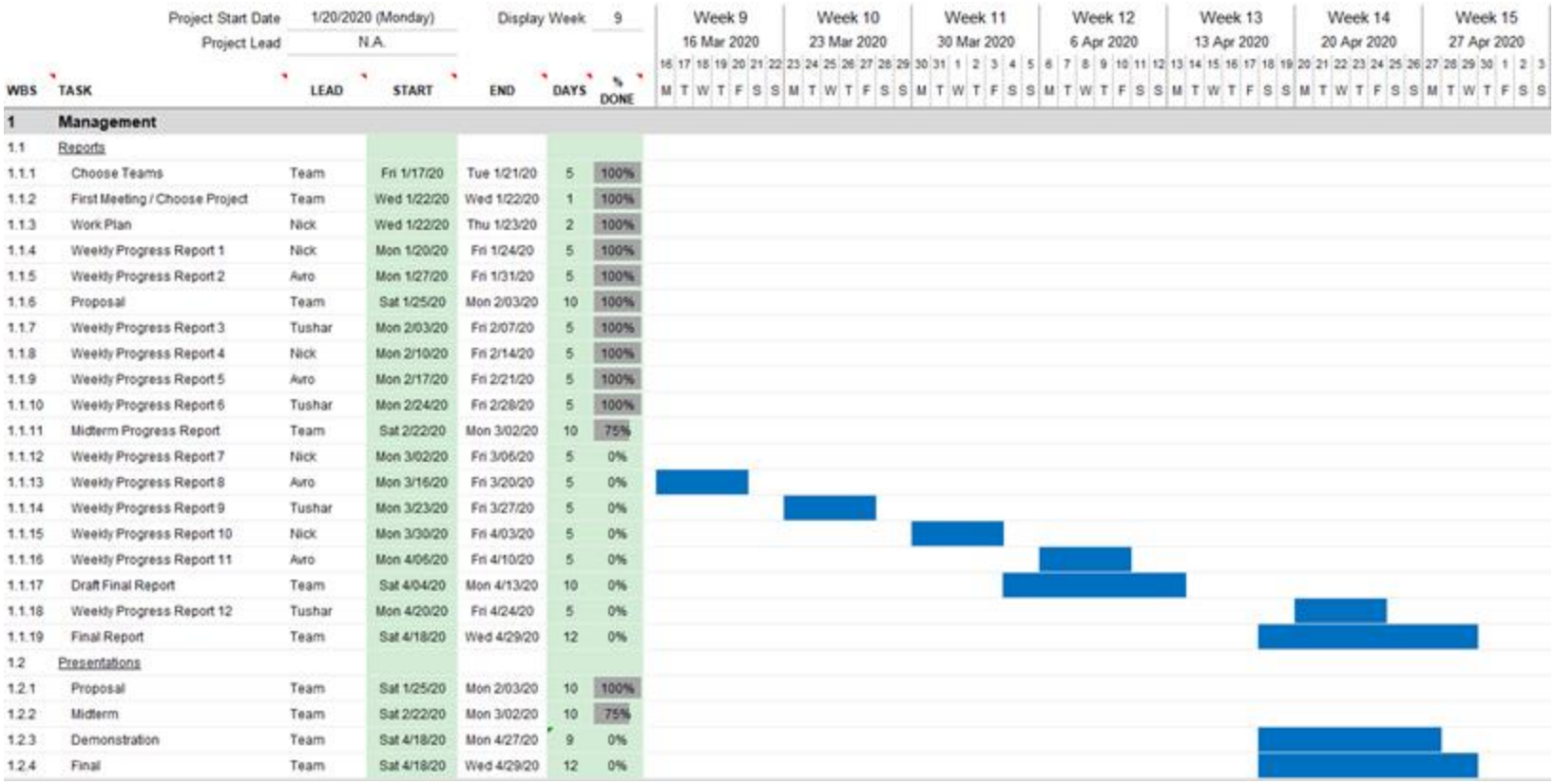

Project Start Date: 1/20/2020 (Monday) | Display Week: 9
Project Lead: N.A.

WBS	TASK	LEAD	START	END	DAYS	% DONE
1	**Management**					
1.1	Reports					
1.1.1	Choose Teams	Team	Fri 1/17/20	Tue 1/21/20	5	100%
1.1.2	First Meeting / Choose Project	Team	Wed 1/22/20	Wed 1/22/20	1	100%
1.1.3	Work Plan	Nick	Wed 1/22/20	Thu 1/23/20	2	100%
1.1.4	Weekly Progress Report 1	Nick	Mon 1/20/20	Fri 1/24/20	5	100%
1.1.5	Weekly Progress Report 2	Avro	Mon 1/27/20	Fri 1/31/20	5	100%
1.1.6	Proposal	Team	Sat 1/25/20	Mon 2/03/20	10	100%
1.1.7	Weekly Progress Report 3	Tushar	Mon 2/03/20	Fri 2/07/20	5	100%
1.1.8	Weekly Progress Report 4	Nick	Mon 2/10/20	Fri 2/14/20	5	100%
1.1.9	Weekly Progress Report 5	Avro	Mon 2/17/20	Fri 2/21/20	5	100%
1.1.10	Weekly Progress Report 6	Tushar	Mon 2/24/20	Fri 2/28/20	5	100%
1.1.11	Midterm Progress Report	Team	Sat 2/22/20	Mon 3/02/20	10	75%
1.1.12	Weekly Progress Report 7	Nick	Mon 3/02/20	Fri 3/06/20	5	0%
1.1.13	Weekly Progress Report 8	Avro	Mon 3/16/20	Fri 3/20/20	5	0%
1.1.14	Weekly Progress Report 9	Tushar	Mon 3/23/20	Fri 3/27/20	5	0%
1.1.15	Weekly Progress Report 10	Nick	Mon 3/30/20	Fri 4/03/20	5	0%
1.1.16	Weekly Progress Report 11	Avro	Mon 4/06/20	Fri 4/10/20	5	0%
1.1.17	Draft Final Report	Team	Sat 4/04/20	Mon 4/13/20	10	0%
1.1.18	Weekly Progress Report 12	Tushar	Mon 4/20/20	Fri 4/24/20	5	0%
1.1.19	Final Report	Team	Sat 4/18/20	Wed 4/29/20	12	0%
1.2	Presentations					
1.2.1	Proposal	Team	Sat 1/25/20	Mon 2/03/20	10	100%
1.2.2	Midterm	Team	Sat 2/22/20	Mon 3/02/20	10	75%
1.2.3	Demonstration	Team	Sat 4/18/20	Mon 4/27/20	9	0%
1.2.4	Final	Team	Sat 4/18/20	Wed 4/29/20	12	0%

Figure 6.2: *Gantt chart of managerial tasks for weeks 9-15.*

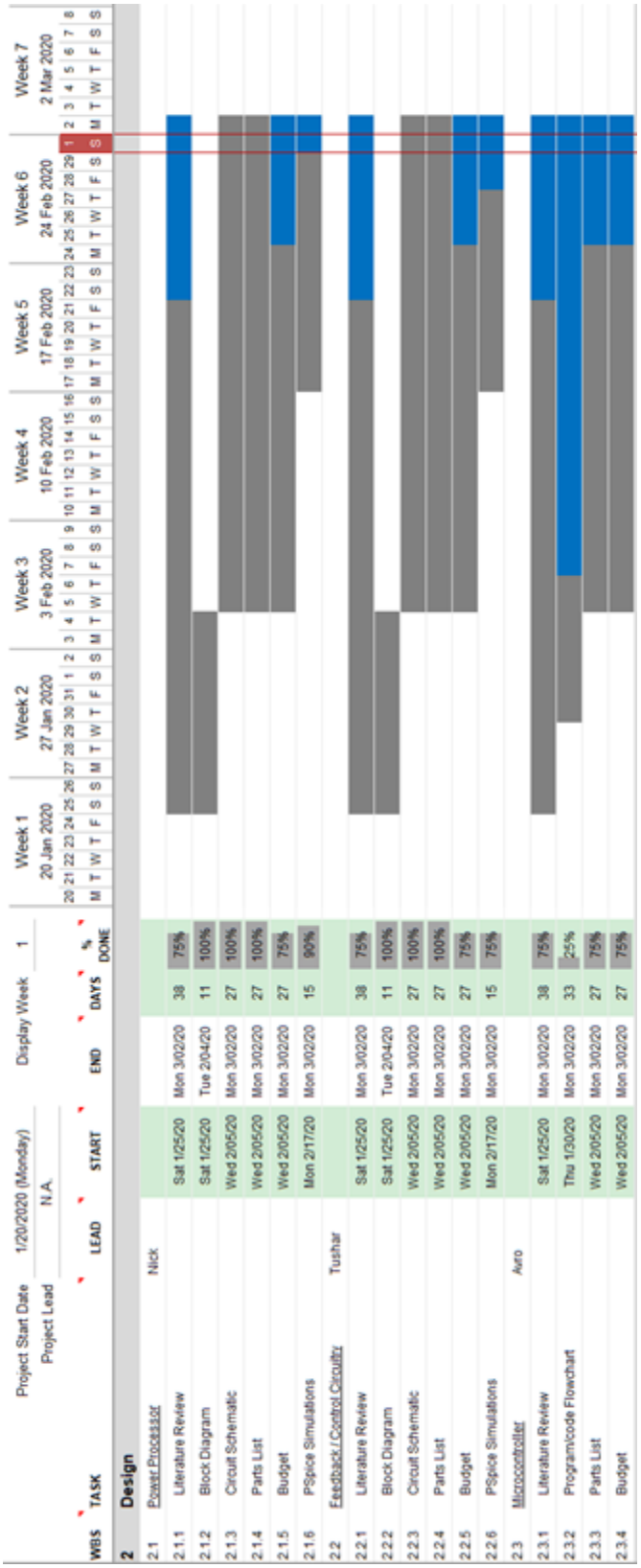

Figure 6.3: *Gantt chart for design related project work.*

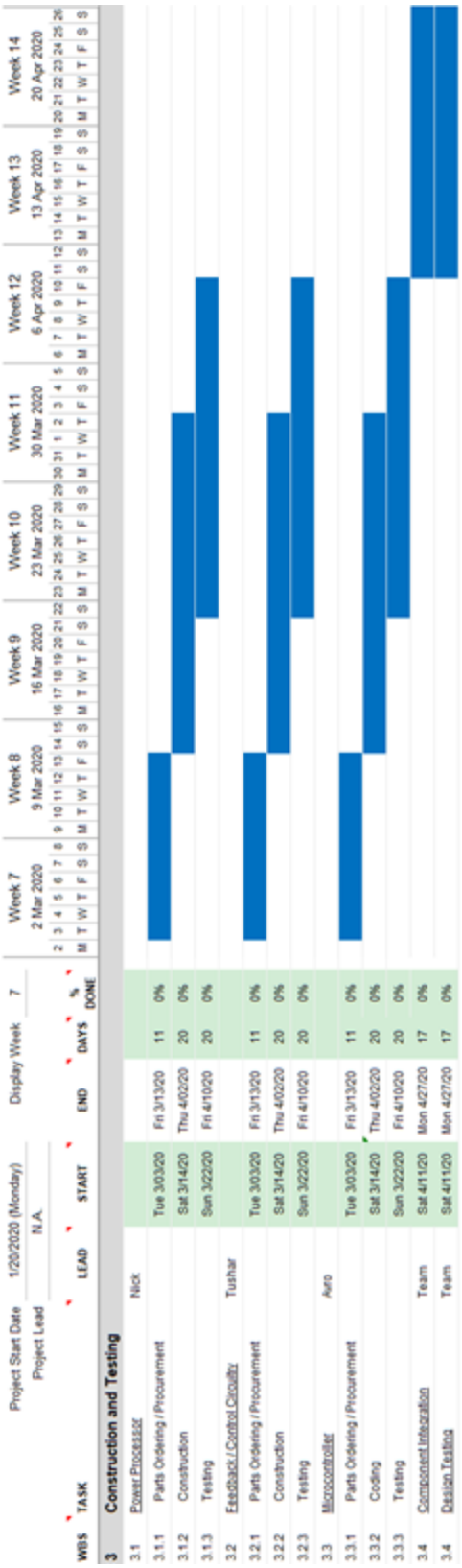

Figure 6.4: *Gantt chart of construction and testing tasks for weeks 9-16.*

6.3. Project Status

As was mentioned, COVID-19 significantly altered plans to complete the project as originally envisioned. Physical realization of the circuit was foregone, and future project plans became to refine and revise system simulations, complete component specifications, and complete project documentation.

We are confident in our component specifications, and feel that we would be unlikely to encounter any specification shortcomings in actual circuit testing of the design. We have simulated our circuit extensively, and have also produced a control algorithm that works well at maintaining a desired output voltage from the buck converters, and have tested this using a modelled solar PV module source. This could be directly translated and implemented in a microcontroller.

Two areas that we feel are relatively weakly simulated or implemented are battery modelling and MPPT implementation. Battery models are complex, and we generally relied on preexisting models which were beyond our immediate understanding. Including the behavior of a charging battery as a load more completely in our simulations may have led to more dynamic circuit behavior. This may be especially true if implementing an MPPT algorithm, and it is in large part the dynamic behavior of a circuit that justifies the use of MPPT.

7. IEEE Code of Ethics Considerations

The IEEE Code of Ethics is familiar to us, and throughout this project we strove to act accordingly. The code of ethical conduct is attached to this document as Appendix A. It is a duly established code of ethics, according to which, we are perpetually expected to behave. In assessing our adherence to the code, we can say that the general public was not exposed to any physically realized system, so concerns for public safety were not existent. Throughout the design process, however, we completed limited laboratory testing of circuitry, and kept our own safety and that of those that came in contact with our design in the laboratory in mind. We had the opportunity to exercise honesty, professionalism and fairness within our team and when representing ourselves. Also, in accordance with the guidelines, we were open to academic criticism, and this allowed us to improve our engineering abilities. We believe that we gave due consideration to the IEEE code, and followed it appropriately.

8. Conclusions

First, to summarize what was accomplished over the course of this project, we were presented with the problem of conditioning the voltage output of a solar PV module to appropriate levels so that it could be safely used to charge 5 V and 12 V batteries. The size of the solar PV module does put practical limitations on the load that could not be overcome by design. If a 12 V battery is connected to the system, this must be the only load given a 12 V batteries charge voltage and currents. Over the allotted design time, we consolidated our understanding of power supplies, and presented a feasible design.

Based on power source and load specifications, we proposed a system with dual buck converters, an advanced microcontroller system, and supporting controls to power converter circuit interfacing elements. While choosing circuit elements we were conscious of past efforts and troubles, and reacted by selecting components with specifications that provide substantial overhead. We were conservative in our selection of switching frequency, and also designed for quality system output signals as low voltage and current ripple as possible. In lieu of testing with a physical circuit prototype, we focused on using simulation to validate our design. We chose MATLAB as a convenient software for simulation, and one that includes many features such as extensive support and libraries with ready-made circuit element models.

We proceeded with simulation in MATLAB® and observed our system operating under different load and input conditions, and validated our design through analysis of transient and steady-state circuit behaviors. In terms of design, we encountered little trouble. A suitable power MOSFET was easy to find, and a simple turn-off snubber circuit was trivial to design and implement to help reduce switching losses and times. As was mentioned, we desired a high quality output signal, and were to a degree forced to this based on charging requirements. Consequently, we would likely have chosen greater inductance and capacitance for the LC filter element of the buck converter had those components been more commonly available. When choosing the inductor, this was especially true, and as we looked at inductors with large inductances we were less and less able to find one with appropriate current ratings.

Initially, we faced a learning curve when transitioning to the MATLAB® simulation environment from the more familiar PSpice one. We also remain unsatisfied with our incorporation of MPPT and battery charge modelling in simulation. With additional time, we would choose to work with the Simscape Electrical battery model in more simple circuits to gain a better understanding of the model, and how to correctly incorporate it within a simulation. Based on the battery specifications that we were able to acquire, we are not aware that a simple resistor

of appropriate value is an invalid approximation of a battery, at least for a short enough duration of time in steady-state operation. On a related note, switching circuits are notoriously difficult to simulate [10], and we found it necessary to utilize small simulation time increments to obtain reasonable results. Consequently, long duration time simulations were, to an extent, infeasible.

With a resistor as a substitute in simulation for a battery load, the utility of an MPPT algorithm may not be as great. The resistor is not a dynamic element, and maximum power occurs at maximum voltage, which is effectively determined by battery specifications and datasheets. Provided the solar PV module can provide at least the minimum power, it is very likely that delivery of maximum power to the load will occur simply by setting a high voltage. MPPT will not impair the behavior of the circuit, but nothing will be gained from it, and we believe this is the behavior we observed during simulation.

In final summary, we have produced a design accompanied by component selection that was validated by MATLAB® and PSpice simulations, and remains ready to be physically implemented and tested in the future.

References

[1] Tamrakar, V., Gupta, S. C., & Sawle, Y. (2015). Single-diode PV cell modeling and study of characteristics of single and two-diode equivalent circuit. *Electrical and Electronics Engineering: An International Journal (ELELIJ)*, *4*(3), 12.

[2] "Arduino Uno Rev3." arduino.cc. https://store.arduino.cc/usa/arduino-uno-rev3 (accessed Apr. 19, 2020).

[3] "Solar Panels Characteristics Current, Voltage, and Power Curves of a Solar (PV) Panel." samlexsolar.com. https://www.samlexsolar.com/learning-center/solar-panels-characteristics.aspx (accessed Apr. 19, 2020).

[4] "Power Electronics Control Design with Simulink." mathworks.com. https://www.mathworks.com/solutions/power-electronics-control/mppt-algorithm.html (accessed Apr. 12, 2020).

[5] Appliance Efficiency Regulations, California Code Of Regulations Title 20, Sections 1601 - 1608. Battery Charger Systems and Self-Contained Lighting Controls. CEC-400- 2012-011-CMF.

[6] R. Kollman and J. Betten, "Powering electronics from the USB port," Texas Instruments Inc., Dallas, TX, USA, 2005. Accessed: Apr. 19, 2020. [Online]. Available: http://www.ti.com/lit/an/slyt118/slyt118.pdf.

[7] https://web.archive.org/web/20131219221448/http://sbrn.solarbuildings.ca/c/sbn/file_db/Doc_File_e/Advanced%20algorithm%20for%20MPPT.pdf

[8] https://www.itacanet.org/eng/elec/battery/battery.pdf

[9] https://www.mathworks.com/matlabcentral/fileexchange/49701-solar-irradiation model?focused=7272110&tab=function

[10] "LTspice." analog.com. https://www.analog.com/en/design-center/design-tools-and-calculators/ltspice simulator.html# (accessed May 1, 2020).

Appendix A: IEEE Code of Ethics

We, the members of the IEEE, in recognition of the importance of our technologies in affecting the quality of life throughout the world, and in accepting a personal obligation to our profession, its members, and the communities we serve, do hereby commit ourselves to the highest ethical and professional conduct and agree:

1. to hold paramount the safety, health, and welfare of the public, to strive to comply with ethical design and sustainable development practices, and to disclose promptly factors that might endanger the public or the environment;
2. to avoid real or perceived conflicts of interest whenever possible, and to disclose them to affected parties when they do exist;
3. to be honest and realistic in stating claims or estimates based on available data;
4. to reject bribery in all its forms;
5. to improve the understanding by individuals and society of the capabilities and societal implications of conventional and emerging technologies, including intelligent systems;
6. to maintain and improve our technical competence and to undertake technological tasks for others only if qualified by training or experience, or after full disclosure of pertinent limitations;
7. to seek, accept, and offer honest criticism of technical work, to acknowledge and correct errors, and to credit properly the contributions of others;
8. to treat fairly all persons and to not engage in acts of discrimination based on race, religion, gender, disability, age, national origin, sexual orientation, gender identity, or gender expression;
9. to avoid injuring others, their property, reputation, or employment by false or malicious action;
10. to assist colleagues and co-workers in their professional development and to support them in following this code of ethics.

Appendix B: Data Sheets

Appendix B.1: Kyocera KC85TS

THE NEW VALUE FRONTIER

KYOCERA

KC85TS

HIGH EFFICIENCY MULTICRYSTAL
PHOTOVOLTAIC MODULE

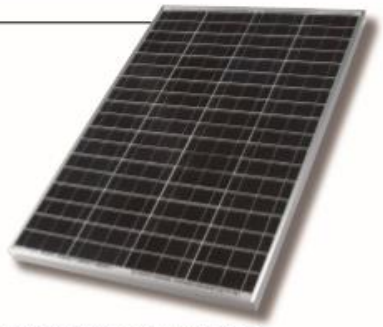

LISTED

HIGHLIGHTS OF KYOCERA PHOTOVOLTAIC MODULES

Kyocera's advanced cell processing technology and automated production facilities produce a highly efficient multicrystal photovoltaic module.
The conversion efficiency of the Kyocera solar cell is over 16%.
These cells are encapsulated between a tempered glass cover and a pottant with back sheet to provide efficient protection from the severest environmental conditions.
The entire laminate is installed in an anodized aluminum frame to provide structural strength and ease of installation.

APPLICATIONS

- Microwave / Radio repeater stations
- Electrification of villages in remote areas
- Medical facilities in rural areas
- Power source for summer vacation homes
- Emergency communication systems
- Water quality and environmental data monitoring systems
- Navigation lighthouses
- Pumping systems for irrigation, rural water supplies and livestock watering
- Aviation obstruction lights
- Cathodic protection systems
- Desalination systems
- Railroad signals
- etc.

QUALIFICATIONS

- **MODULE** : UL1703 certified
  Hazardous Locations Class I, Div 2, Groups A, B, C and D
- **FACTORY** : ISO9001 and ISO 14001

QUALITY ASSURANCE

Kyocera multicrystal photovoltaic modules have passed the following tests.

- Thermal cycling test
- Thermal shock test
- Thermal / Freezing and high humidity cycling test
- Electrical isolation test
- Hail impact test
- Mechanical, wind and twist loading test
- Salt mist test
- Light and water-exposure test
- Field exposure test

LIMITED WARRANTY

※1 year limited warranty on material and workmanship
※20 years limited warranty on power output: For detail, please refer to "category IV" in Warranty issued by Kyocera

(Long term output warranty shall warrant if PV Module(s) exhibits power output of less than 90% of the original minimum rated power specified at the time of sale within 10 years and less than 80% within 20 years after the date of sale to the Customer. The power output values shall be those measured under Kyocera's standard measurement conditions. Regarding the warranty conditions in detail, please refer to Warranty issued by Kyocera)

ELECTRICAL CHARACTERISTICS

Current-Voltage characteristics of Photovoltaic Module KC85TS at various cell temperatures

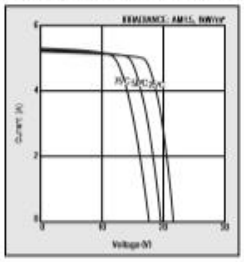

Current-Voltage characteristics of Photovoltaic Module KC85TS at various irradiance levels

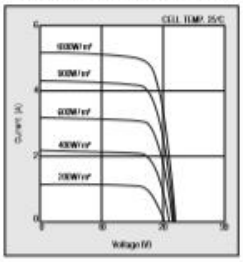

SPECIFICATIONS

KC85TS

■ Physical Specifications

Unit : mm (in.)

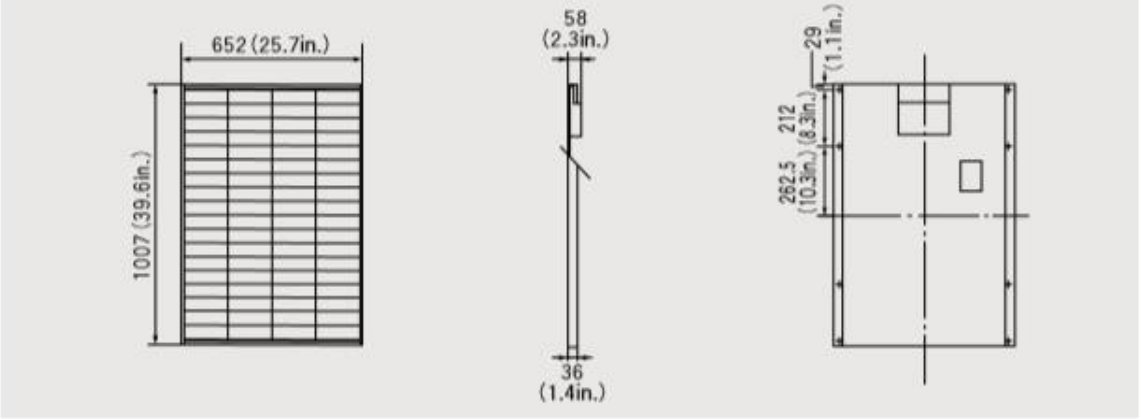

■ Specifications

■ Electrical Performance under Standard Test Conditions (*STC)	
Maximum Power (P_{max})	87W (+10%/−5%)
Maximum Power Voltage (V_{mpp})	17.4V
Maximum Power Current (I_{mpp})	5.02A
Open Circuit Voltage (V_{oc})	21.7V
Short Circuit Current (I_{sc})	5.34A
Max System Voltage	600V
Temperature Coefficient of Voc	-8.21×10^{-2} V/℃
Temperature Coefficient of Isc	2.12×10^{-3} A/℃

*STC : Irradiance 1000W/m², AM1.5 spectrum, module temperature 25℃

■ Electrical Performance at 800W/m², NOCT, AM1.5	
Maximum Power (P_{max})	62W
Maximum Power Voltage (V_{mpp})	15.3V
Maximum Power Current (I_{mpp})	4.06A
Open Circuit Voltage (V_{oc})	19.7V
Short Circuit Current (I_{sc})	4.31A

NOCT (Nominal Operating Cell Temperature) : 47℃

■ Cells	
Number per Module	72

■ Module Characteristics	
Length × Width × Depth	1007mm(39.6in.)×652mm(25.7in.)×58mm(2.3in.)
Weight	8.3kg(18.3lbs.)

■ Junction Box Characteristics	
Length × Width × Depth	170.6mm(6.7in.)×101.6mm(4.0in.)×31.9mm(1.3in.)
IP Code	IP65

■ Reduction of Efficiency under Low Irradiance	
Reduction	6.1%

Reduction of efficiency from an irradiance of 1000W/m² to 200W/m² (module temperature 25℃)

Please contact our office for further information

KYOCERA

KYOCERA Corporation

■ KYOCERA Corporation Headquarters
CORPORATE SOLAR ENERGY DIVISION
6 Takeda Tobadono-cho
Fushimi-ku, Kyoto
612-8501, Japan
TEL:(81)75-604-3476 FAX:(81)75-604-3475
http://www.kyocera.com

● KYOCERA Solar, Inc.
7812 East Acoma Drive
Scottsdale, AZ 85260, USA
TEL:(1)480-948-8003 or (800)223-9580 FAX:(1)480-483-6431
http://www.kyocerasolar.com

● KYOCERA Solar do Brasil Ltda.
Av. Gangard 661, Loja A
22790-200, Recreio dos Bandeirantes, Rio de Janeiro, Brazil
TEL:(55)21-2437-8525 FAX:(55)21-2437-2338
http://www.kyocerasolar.com.br

● KYOCERA Solar Pty Ltd.
Level 3, 6-10 Talavera Road, North Ryde
N.S.W. 2113, Australia
TEL:(61)2-9870-3948 FAX:(61)2-9888-9588
http://www.kyocerasolar.com.au/

● KYOCERA Fineceramics GmbH
Fritz-Mueller-Strasse 107, 73730 Esslingen, Germany
TEL:(49)711-93934-999 FAX:(49)711-93934-950
http://www.kyocerasolar.eu

● KYOCERA Asia Pacific Pte. Ltd.
298 Tiong Bahru Road, #13-03/05
Central Plaza, Singapore 168730
TEL:(65)6271-0500 FAX:(65)6271-0600

● KYOCERA Asia Pacific Ltd.
Room 801-802, Tower 1 South Seas Centre, 75 Mody Road,
Tsimshatsui East, Kowloon, Hong Kong
TEL:(852)2-7237183 FAX:(852)2-7244501

● KYOCERA Asia Pacific Ltd. Taipei Office
10 Fl., No.66, Nanking West Road, Taipei, Taiwan
TEL:(886)2-2555-3600 FAX:(886)2-2550-4131

● KYOCERA(Tianjin) Sales & Trading Corporation
10F, Tower C HeQiao Building 8A Guanghua Rd.,
Chao Yang District, Beijing 100026, China
TEL:(86)10-6583-2270 FAX:(86)10-6583-2250

Kyocera reserves the right to modify these specifications without notice

LIE/A0080704-SAGM

Appendix B.2: UB12180 (12 Volt Lead-Acid Battery)

UPG
STAY POWERED

Sealed Lead-Acid Battery

UPG No. 40648

UB12180

Maintenance-Free

Absorbant Glass Mat (AGM) technology for superior performance. Valve regulated, spill proof construction allows safe operation in any position. Approved for transport by air. D.O.T., I.A.T.A., F.A.A. and C.A.B. certified. U.L. r ecognized under file number MH 20567.

Specification

Nominal Voltage	12 volts
Nominal Capacity	77° F (25° C)
20-hr. (0.90A)	18 Ah
10-hr. (1.67A)	16.74 Ah
5-hr. (3.06A)	15.30 Ah
1-hr. (10.80A)	10.80 Ah
Approximate Weight	11.9 lbs (5.4 kgs)
Internal Resistance (approx.)	18mΩ

Shelf Life (% of normal capacity at 77° F (25° C))

3 Months	6 Months	12 Months
91%	82%	64%

Temperature Dependancy of Capacity (20 hour rate)

104° F (40°C)	77° F (25°C)	32° F (0°C)	5° F (-15°C)
102%	100%	85%	65%

AGM Operational Temperature	
Charge	32°F to 104°F (0°C to 40°C)
Discharge	5°F to 113°F (-15°C to 45°C)
AGM Storage Temperature	5°F to 104°F (-15°C to 40°C)

*Can be used outdoors.

Charge Method (Constant Voltage)	
Cycle Use (Repeating Use)	
Initial Current	5.4 A or smaller
Control Voltage	14.6 - 14.8 V
Float Use	
Control Voltage	13.6 - 13.8 V

Physical Dimensions: in (mm)

L: 7.13in (181.1 mm)
W: 3.01in (76.5 mm)
H: 6.50in (165.1 mm)
TH: 6.57in (166.9 mm)
Tolerances are +/- 0.04 in. (+/- 1mm) and +/- 0.08 in. (+/- 2mm) for height dimensions. All data subject to change without notice.

Terminals

Type	L	B	a	H	T
F2	7.80 mm 0.31 in	6.35 mm 0.25 in	7.80 mm 0.31 in	6.00 mm 0.24 in	0.80 mm 0.03 in

Discharge Time vs. Discharge Current

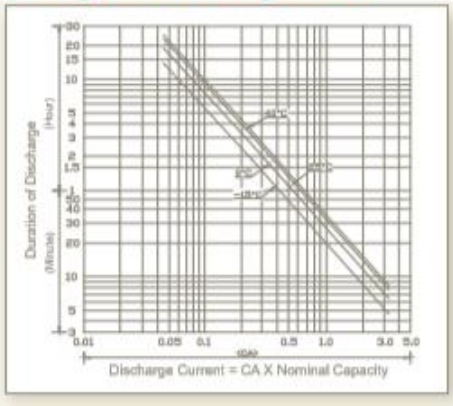

Discharge Characteristics

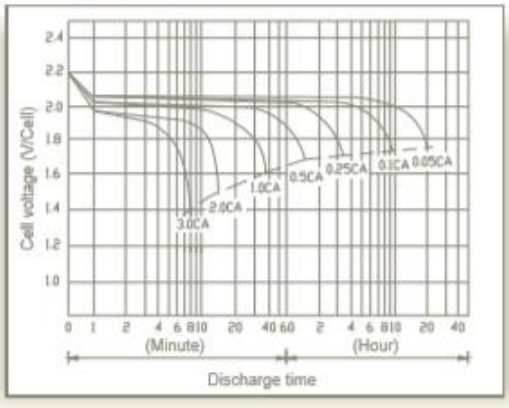

www.upgi.com

ISO 9001 :2008

488 S. Royal Lane | Coppell, Texas 75019 | P 469.892.1122 | T 866.892.1122 | F 469.892.1123 | sales@upgi.com

D1331-1

Shelf Life & Storage

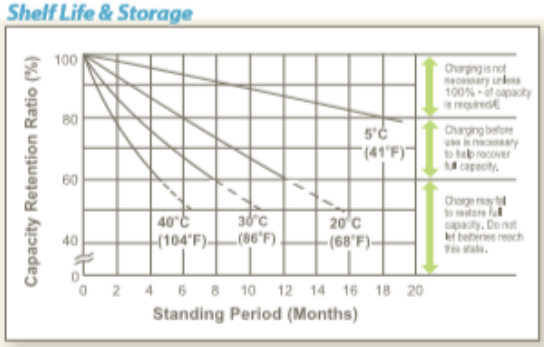

Cycle Life vs Depth of Discharge

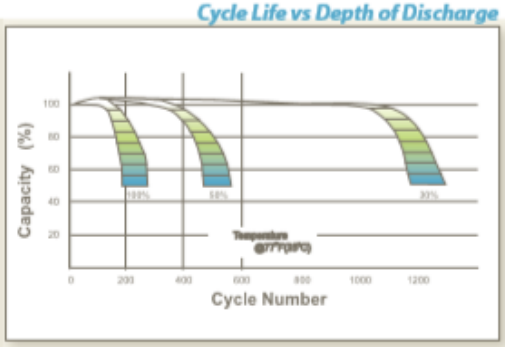

Open Circuit Voltage vs Residual Capacity

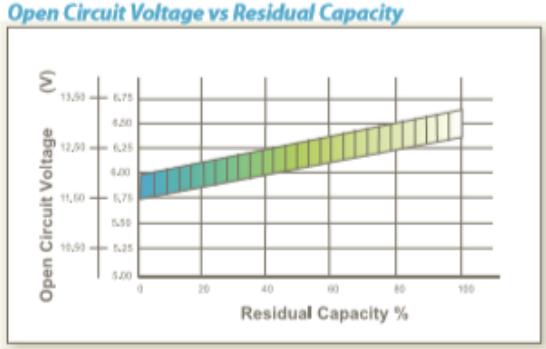

Effect of Temperature on Capacity

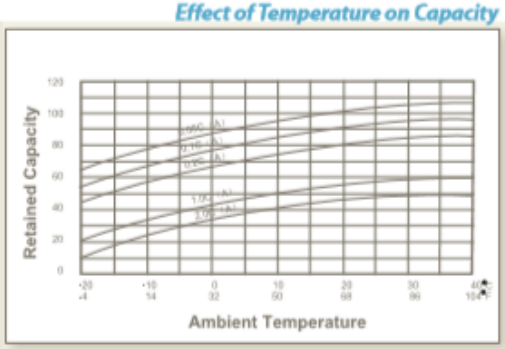

Charge Current & Final Discharge Voltage

Application	Charge Voltage(V/Cell)			Max.Charge Current
	Temperature	Set Point	Allowable Range	
Cycle Use	25℃(77℉)	2.45	2.40~2.50	0.30*C
Standby	25℃(77℉)	2.30	2.27~2.30	

Final Discharge Voltage V/Cell	1.75	1.70	1.60	1.30
Discharge Current(A)	0.2C>(A)	0.2C<(A)<0.5C	0.5C<(A)<1.0C	(A)>1.0C

Appendix B.3: Arduino Uno Rev3

Microcontroller	ATmega328P
Operating Voltage	5V
Input Voltage (recommended)	7-12V
Input Voltage (limit)	6-20V
Digital I/O Pins	14 (of which 6 provide PWM output)
PWM Digital I/O Pins	6
Analog Input Pins	6
DC Current per I/O Pin	20 mA
DC Current for 3.3V Pin	50 mA
Flash Memory	32 KB (ATmega328P) of which 0.5 KB used by bootloader
SRAM	2 KB (ATmega328P)
EEPROM	1 KB (ATmega328P)
Clock Speed	16 MHz
LED_BUILTIN	13
Length	68.6 mm
Width	53.4 mm
Weight	25 g

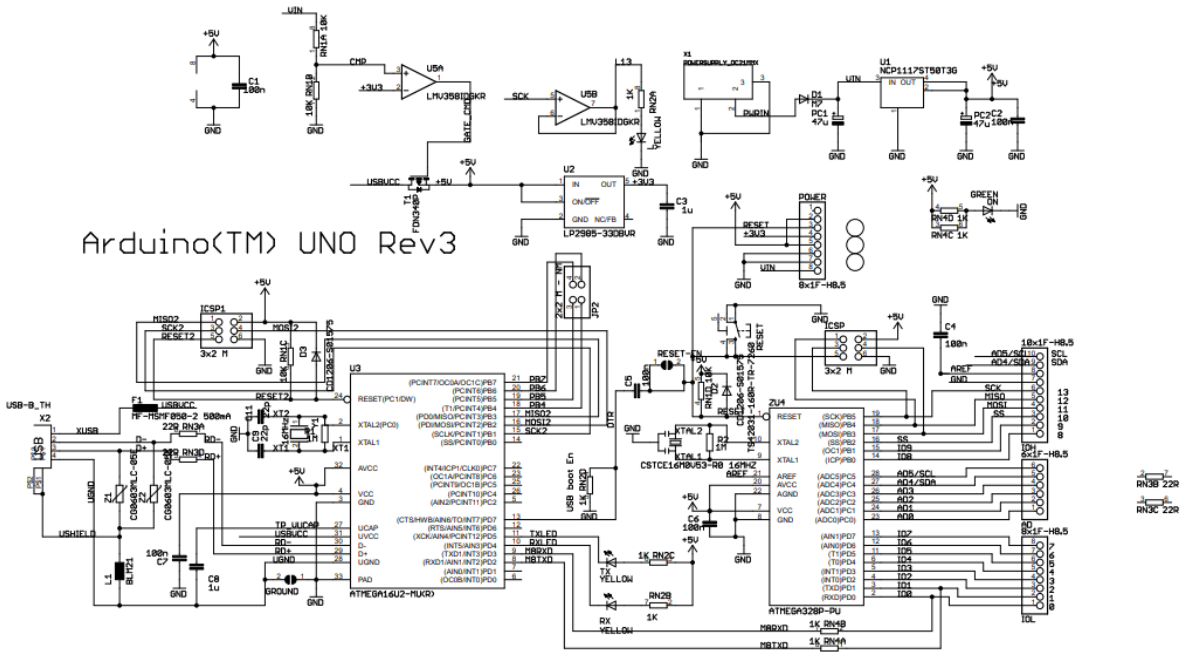

Appendix B.4: Pololu 7.5 (D24V22F7) Regulator

Dimensions

Size:	0.7″ × 0.7″ × 0.31″[1]
Weight:	2.3 g[1]

General specifications

Minimum operating voltage:	8.0 V[2]
Maximum operating voltage:	36 V
Continuous output current:	2 A[3]
Output voltage:	7.5 V
Reverse voltage protection?:	Y
Maximum quiescent current:	3 mA[4]

Identifying markings

PCB dev codes:	reg19a
Other PCB markings:	0J9251

Appendix B.5: Additional Components

Please see the attached file for additional component datasheets that would be excessively large to incorporate in this report.

Appendix C: MPPT Tracking Simulation Diagram